LU TP 95-13
September 1995
revised

The Linked Dipole Chain Model for DIS

B. Andersson [1], G. Gustafson [2], J. Samuelsson [3]

Department of Theoretical Physics
Lund University
Sölvegatan 14A
S-223 62 Lund, Sweden

Abstract

The Linked Dipole Chain Model provides an interpolation between the regions of high Q^2 (DGLAP) and low x-moderate Q^2 (BFKL) in DIS. It is a reformulation and a generalization of the results obtained by Ciafaloni, Catani, Fiorani and Marchesini, and it gives a unified treatment of "normal DIS", boson-gluon fusion events and hard subcollisions in resolved photon-proton scattering. Thus the formalism provides a complete picture which incorporates all hard or semi-hard hadronic interactions in a simple way, which is suitable for a Monte Carlo treatment of both structure functions and final state properties. We also discuss nonleading effects which significantly reduce the increase of the structurefunction for very small x-values.

[1]bo@thep.lu.se (internet)
[2]gosta@thep.lu.se(internet)
[3]jim@thep.lu.se (internet)

1 Introduction

Gribov and his collaborators, [1], considered the results of the resummation of the high order perturbation terms in general field theories and obtained the Leading Log (LLA) (and later the Modified Leading Log, (MLLA)) Approximations. The moment equations, [2], stemming from investigations of the lightcone singularities of the field theories, turned out to give equivalent results at least for QCD, [3]. The whole procedure to obtain the structure functions f is nowadays usually formulated in terms of the DGLAP equations:

$$\frac{\partial F(x,Q^2)}{\partial \log(Q^2)} = \int_x^1 dz \frac{\alpha_s}{2\pi} P(z) F(x/z, Q^2) \tag{1}$$

where P is the splitting funtion regularized at $z = 1$. Actually this is a matrix equation for the structure functions for different quanta, with different splitting function P contributions for the different processes $g \to gg$ (g stands for the color-8 gluons), $q \to qg$ (q ($\bar{q}$) stands for the color 3 quarks ($\bar{3}$ antiquarks)) and $g \to q\bar{q}$. These "evolution equations" are stable for evolution "forwards", ie towards large Q^2-values.

In the DGLAP approach the final Q^2-value is assumed to be very large and the dominating contributions come from development chains where the transverse momenta in the emissions are strongly ordered along the chain (cf fig 1) towards this large Q^2. Therefore, if the transverse momenta in a splitting are called $\vec{k}'_\perp \to (\vec{k}_\perp, \vec{q}_\perp)$ (with $\vec{k}_\perp = \vec{k}'_\perp - \vec{q}_\perp$) in easily understood notations then $(\vec{k}_\perp)^2 \gg (\vec{k}'_\perp)^2$. In this way the value of $(\vec{q}_\perp)^2$ dominates the earlier emissions and equals the corresponding $(\vec{k}_\perp)^2$-value and it means in particular that in each step the largest values of $\vec{k}_\perp^2$ dominates and the transverse momentum dependence may then be treated by the derivative in eq (1).

The basic finding for the BFKL approach, [4] , which is meant to be relevant for small x and moderate Q^2, is that there are many more configurations possible if the transverse momenta in the emissions are allowed both to increase and decrease along the chain. The resulting equation is then more complex and in particular contains a kernel-function K for the transfer from the value $\vec{k}'_\perp$ to $\vec{k}_\perp$ in each emission. It is the largest eigenvalue, λ, of this kernel which occurs in the power law behaviour $x^{-\lambda}$ predicted in the BFKL approach for small values of the Bjorken variable x.

Both of the approaches mentioned above are meant to describe the properties of the structure functions but none of them is directly suitable to obtain the exclusive states including the radiation. It is then necessary to obtain a formulation incorporating both the region of small and large values of (x, Q^2) and at the same time be able to consider the exclusive final states. Such a description which interpolates between DGLAP and BFKL is presented by Ciafaloni and Catani et al. [5, 6] in a general approach for the resummation of the higher order perturbative corrections stemming from multiple gluon emission.

We will in this paper reformulate and generalize their results in such a way that we obtain a unified treatment of "normal DIS", boson-gluon fusion events and high-$p_\perp$ resolved photon interaction. The formalism can also be used for hard hadronic collisions and $\gamma\gamma$-interactions.

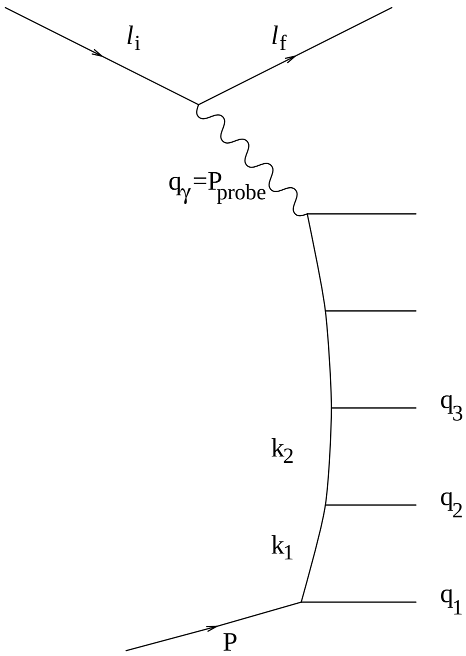

Figure 1: *A DIS fan diagram.*

We formulate the results in the language of the color dipole model, [7], developed for e^+e^--annihilation and implemented in the Ariadne MC [8]. The dipole model takes automatically into account the angular ordering due to soft gluon coherence and for DIS this formulation provides an intuitive picture in terms of a chain of linked dipoles. This chain is formed in accordance with a stochastic process containing the color coherence conditions. The dipole chain specifies the total final state, and the process is suitable for MC simulations both of the structure functions and of the properties of the final states. Such a Monte Carlo procedure will be presented later.

In section 2 of this paper we discuss the DGLAP and BFKL procedures in more detail. We end by showing that although the BFKL kernel function and its eigenvalues are very stable, nonleading kinematical constraints will mean a large decrease in the power λ. This is analogous to results for e^+e^--annihilation where nonleading terms are known to give significant modifications, [9]. In section 3 we will provide a brief introduction to multiple gluon emission in the Dipole Cascade Model (DCM) approximation for e^+e^--annihilation and the Webber-Marchesini Cascade Model. We also present some remarks on the properties of Sudakov formfactors which occur in connection with exclusive states.

In section 4 we will consider the approach of ref [6] to describe the states of DIS. We reformulate their results in terms of the color dipole model and demonstrate that it can be interpreted in terms of a chain of linked dipoles. In section 5 we generalize their results to include boson-gluon fusion and high-$p_\perp$ parton-parton scattering, and discuss subleading contributions and the probe and target ends of the perturbative chain.

Finally in section 6 we derive an equation for the structure functions of a hadron, which incorporates both the DGLAP and the BFKL parts, but nevertheless is different from each and also different from the results of ref [6]. We trace the differences in some detail and we calculate the so-called anomalous dimensions, ie the leading power behaviour of the solutions. We again find an essential decrease compared to the BFKL exponent, this time due to different reasons, however.

2 The DGLAP and BFKL mechanisms.

We will start to consider the properties of eq (1) and then we go over to a treatment of the BFKL mechanism.

The main behaviour of the gluon structure functions F_g in eq (1) can be obtained from the following considerations (somewhat vulgarized compared to the original arguments, [10]). Consider the (repeated) emission(s) $g_0 \rightarrow g_1 g_2$ (which are the dominating ones) with the kinematics that g_0 has a lightcone fraction x_0 and a transverse momentum $\vec{k}'_\perp$ and g_1 (g_2) correspondingly $(x_1 = x_0 z, \vec{k}_\perp = \vec{k}'_\perp - \vec{q}_\perp)$ $((x_0(1-z), \vec{q}_\perp))$.

We follow the z-splittings, and note that in the DGLAP approach the transverse momenta are increasing along this parton line, ie $(\vec{k}_\perp)^2 \gg (\vec{k}'_\perp)^2$ up towards the (very large) value Q^2. This means that each $\vec{q}_\perp^2$ dominates the earlier ones and (on the logarithmic scale we are in practice using) it is equal to the corresponding $\vec{k}_\perp^2$-value. Then the derivative of F_g can be written as an iteration. Also the energies are strongly ordered, and therefore we will in the gluon emission only retain the z-pole, ie we use

$$\frac{\alpha_s}{2\pi} P_{g \rightarrow gg} \simeq \bar{\alpha} \frac{1}{z(1-z)} \simeq \bar{\alpha} \frac{1}{z} \tag{2}$$

with $\bar{\alpha}$ the effective coupling constant, for the gluon emission $\bar{\alpha} = 3\alpha_s/\pi$. Summing the number of connected gluon "roads", ie connected emissions $g \rightarrow gg$, we obtain the following result for the structure function for the gluon, F_g, which is related to the gluon density

$$\begin{aligned} \frac{\partial F_g}{\partial \log(Q^2/k_{\perp 0}^2)} \equiv \frac{\partial^2 n_g}{\partial \log(Q^2/k_{\perp 0}^2) \partial \log(1/x)} = \sum_n \int \prod_{i=1}^n \bar{\alpha} \frac{dz_i}{z_i} \frac{dk_{\perp i}^2}{k_{\perp i}^2} \times \\ \delta\left(\sum_{i=1}^n \log(1/z_i) - \log(1/x)\right) \cdot \delta\left(\sum_{i=1}^n \log(k_{\perp i}^2/k_{\perp(i-1)}^2) - \log(Q^2/k_{\perp 0}^2)\right) \end{aligned} \tag{3}$$

Using the well-known formula (valid for positive y_i-values)

$$\int \prod_{i=1}^n dy_i \delta\left(\sum_{i=1}^n y_i - Y\right) = \frac{Y^{n-1}}{(n-1)!} \tag{4}$$

one obtains for $f = \frac{\partial F}{\partial \log(Q^2)}$ the result

$$f_{gDGLAP} \propto \sum_n \frac{(\log(1/x)\chi(Q^2))^n}{(n!)^2} \propto \exp\left[2\sqrt{\chi(Q^2)\log(1/x)}\right] \tag{5}$$

with $\chi = \int_{k_{\perp 0}^2}^{Q^2} \bar{\alpha} dk_\perp^2/k_\perp^2$. The scale $k_{\perp 0}^2$ then corresponds to the original parton "virtuality".

The main point is that there is a double iteration both in the splitting variables z and in the increasing transverse momenta, which results in the squared factorial. Due to the properties of the running coupling constant the Q^2-dependence is very weak, $\chi \sim \log(\log(Q^2))$, and the squared factorial implies that the x dependence for small x-values is slower than any power.

In the BFKL approach it is noted that for modest Q^2-values there will be many more contributions in case one allows both an increase and a decrease in the transverse momenta. However, it is necessary to use a more complex kernel, K, so that the n:th step in the transverse momentum $\vec{k}'_\perp \to \vec{k}_\perp$ results from:

$$f_n(\vec{k}_\perp^2) = \int d(\vec{k}'_\perp)^2 K(\vec{k}_\perp^2, \vec{k}_\perp'^2) f_{n-1}(\vec{k}_\perp'^2) \tag{6}$$

In order to find the results of this approach it is necessary to obtain the eigenvalues of the kernel K (we consider the equation later again in section 6). In particular the largest eigenvalue turns out to be $\lambda = 12\alpha_s \log(2)/\pi$ (for a fixed coupling constant α_s). This means that in the n:th iteration the contribution from the DGLAP eq (5) is changed so that

$$\frac{\chi(Q^2)^{(n-1)}}{(n-1)!} \to \lambda^n \tag{7}$$

In this way the square-root in the exponential in eq (5) is also changed:

$$f_{gBFKL} \propto \sum_n \frac{(\lambda \log(1/x))^n}{n!} \simeq \exp(\lambda \log(1/x) = x^{-\lambda} \tag{8}$$

ie the BFKL result corresponding to a positive $1/x$-power. We note that the important point is the exchange of an iterated integral into a plain number obtained in every iteration. The integration will always win out in the asymptotic limit when Q^2 is sufficiently large, but the power will be relevant for smaller values of Q^2.

The kernel K in the BFKL approach is singular if the coupling constant is allowed to run. Allowing that would, however, not be consistent in the present scheme because the BFKL approach was never intended to cover such corrections. The BFKL kernel, K, and its eigenvalues turn out to be very stable (for a constant coupling) against perturbations of the procedure. One may imagine that the (logarithmic) "steps" in the integration variable should be made into discrete steps (for a motivation, cf ref [11],[12]) so that the eq (6) becomes a sum. This is easily doable but the results only correspond to tiny changes in the value of λ. Mueller, [13], has also considered the production process in the transverse coordinate space and again obtains the BFKL eigenvalues from these "transverse" contributions.

We will end this section with a remark to indicate that the BFKL-results nevertheless are rather unstable *with respect to nonsingular terms in the z-dependence of the iteration.* One feature which is essential in the BFKL approach is that in every splitting $k' \to k + q$ the virtual gluon propagator contains only a *small fraction of the energy-momentum*, while most of this energy-momentum, the fraction $(1 - z)$, is carried away by the emitted gluon q

(we have conventionally followed the z-pole contributions and in Mueller's treatment it is the "rapidity"). It is then necessary for consistency to demand that z is small, ie in this convention that $z < \exp(-a)$ for some real number a (which must be at least $a > \log(2)$ in order that $z < (1-z)$). (Another argument would be to say that unless we restrict the z-variations, we are breaking energy-momentum conservation along the emission).

If we introduce a simple restriction in the integration domain, we obtain the following modification to eq (4)

$$\int \prod_{i=1}^{n} dy_i \delta \left(\sum_{i=1}^{n} y_i - Y \right) \rightarrow \int \prod_{i=1}^{n} dy_i \delta \left(\sum_{i=1}^{n} y_i - (Y - na) \right) = \frac{(Y-na)^{n-1}}{(n-1)!} \tag{9}$$

(keeping to the notations in eqs (3) and (4)). Thus we will no longer obtain the BFKL exponent. It is straightforward, using the Stirling approximation to the factorial to obtain the change to eq (8) as a power in $1/x$ with $\lambda \rightarrow \rho$ with the relation $\log(\lambda/\rho) = a\rho$. Thus the power λ is diminished so that $\lambda \rightarrow \rho \simeq \lambda(1 - a\lambda)$.

We conclude that the BFKL mechanism obtains a large part of its contributions from the possibility to emit gluons with small $(1-z)$-value. This decrease in the exponent is also found in a consistent evaluation of the precise structure function, cf ref [12]. We note that the correction exhibited above is of the order α_s^2 (which is expected in the BFKL treatment), but it should also be noted that the correction is very large! We will return to these nonleading effects in section 6.

3 Parton Cascades in e^+e^--Annihilation

We start with a brief description of multiple gluon emission in "time-like" cascades in e^+e^--annihilation events in order to present a scenario useful for the further considerations of the space-like cascades occurring in DIS. In the next subsection we compare to the Webber-Marchesini cascades in order to show the similarity between the two conceptually very different approaches to time-like cascades. We end with a few remarks on the Sudakov formfactors.

3.1 Gluon Emission in the Dipole Cascade Model

Consider an initial (color singlet) $q\bar{q}$-state. At high energies this state will emit gluons by color dipole radiation in accordance with the well-known formula:

$$dp = \frac{C\alpha_s}{2\pi} dx_1 dx_3 \frac{(x_1^2 + x_3^2)}{(1-x_1)(1-x_3)} \tag{10}$$

Here C is a color factor ($C = 4/3$ for a $q\bar{q}$-dipole), α_s the coupling constant and x_j the cms energy fractions of the final state partons with the emitted gluon x_2 fulfilling $x_2 + x_1 + x_3 = 2$.

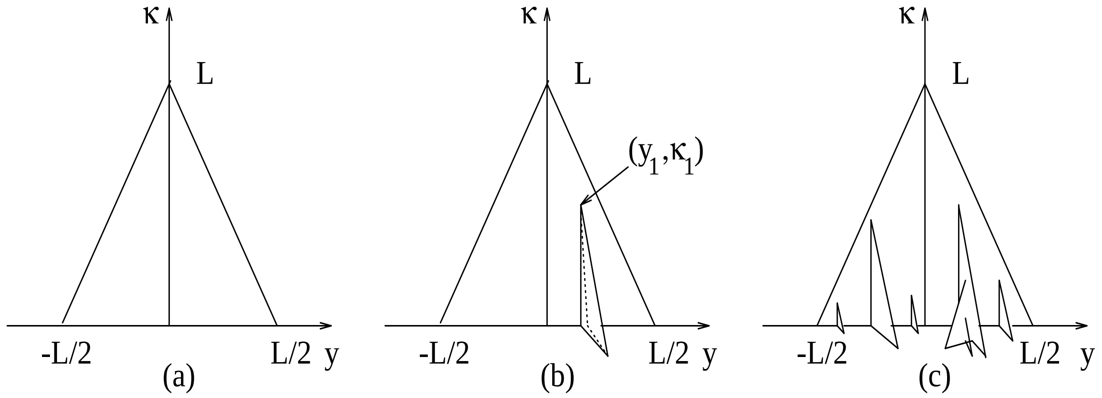

Figure 2: *(a) The phase space available for a gluon emitted by a high energy $q\bar{q}$ system is a triangular region in the y-κ plane. (b) If one gluon is emitted at (y_1, κ_1) the phase space for a second (softer) gluon is represented by the area of this folded surface. (c) Each emitted gluon increases the phase space for the softer gluons. The total gluonic phase space can be described by this multifaceted surface.*

We note in passing that the mass squares of the parton pairs (qg) $(s_{12} = W^2(1-x_3))$ and $(g\bar{q})$ $(s_{23} = W^2(1-x_1))$ are expressible in terms of the original dipole mass W and the x_j's.

It is convenient to introduce the Lorentz invariant transverse momentum and rapidity

$$k_\perp^2 = W^2(1-x_1)(1-x_3) \quad \text{and} \quad y = \frac{1}{2}\log\left(\frac{1-x_1}{1-x_3}\right) \tag{11}$$

and in terms of them we have for the cross section $(x_1 \simeq x_3 \simeq 1)$

$$dp \simeq \frac{C\alpha_s}{\pi}\frac{dk_\perp^2}{k_\perp^2}dy \tag{12}$$

For the phase space we have in the cms of the dipole

$$k_\perp \cosh(y) \leq \frac{W}{2} \tag{13}$$

which can be conveniently approximated by

$$k_\pm \equiv k_\perp \exp(\pm y) < W \tag{14}$$

corresponding to a triangular region in the $(y, \kappa \equiv \ln(k_\perp^2))$-plane, cf fig 2a.

The formula is besides the color factor the same as the one obtained in QED but in this case there is a major change in the final state. Emitting a photon in QED does not change the current. But in QCD the current is changed because the emitted gluon is an octet and therefore the final state contains a color 3 (the q), an $\bar{3}$ (the $\bar{q}$) and the 8-gluon. There is, however, the simplification that instead of forming a complex charge system, the three final state partons form *two independent dipoles*, [14]. Thus if we consider the emission of two gluons, indexed 1 and 2, where $k_{\perp 1} \geq k_{\perp 2}$, the cross section is factorisable into

$$dp(q\bar{q} \to qg_1g_2\bar{q}) = dp(q\bar{q} \to qg_1\bar{q})(dp(qg_1 \to qg_2g_1) + dp(g_1\bar{q} \to g_1g_2\bar{q})) \tag{15}$$

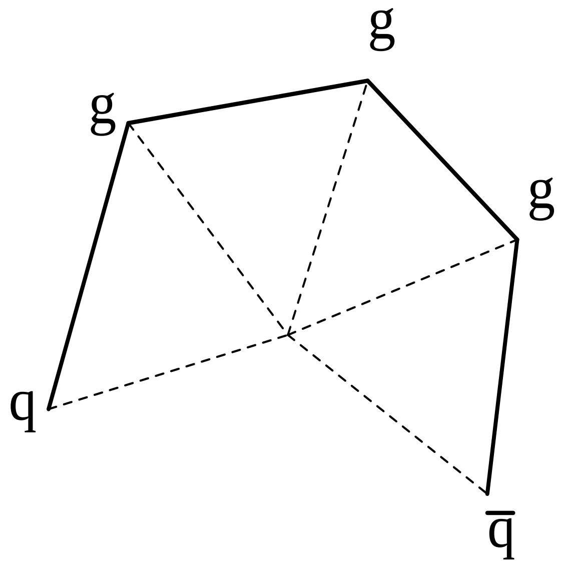

Figure 3: *The dipoles connect the quarks and gluons in the same way as the string in the Lund string fragmentation model.*

where all the terms dp on the right hand side have the form given in eq (12). This factorisation property is better than a few percent all over the phase space, [15]. We note in particular that the two dipoles are not at rest with respect to each other or the original cms.

The DCM is then based upon the production of one dipole $\rightarrow$ two dipoles $\rightarrow$ three...etc. Every time a new gluon is emitted and the corresponding dipole partitioned. Actually the final state containing a set of dipoles has a strong similarity to the Lund String with a set of gluon excitations dragging out a set of straight string segments (corresponding to the dipoles), cf fig 3. As the masses of the dipoles quickly diminish, the corresponding gluons quickly become soft, ie the excitations on the string become smaller and smaller.

A general rule in string fragmentation is that a gluon with less than a few GeV of transverse momentum does no longer really produce any noticable effects. There is no "extra" particle production and the transverse momentum given away by the gluon to the string neighbourhood is drowning in the background noice. Therefore adding to the cascade the use of Lund string fragmentation means that the whole process is infrared stable. The Dipole Cascade Model is implemented as a Monte Carlo simulation process in ARIADNE, [8].

It is useful to note that one gluon emission actually increases the phase space for further emissions. While the cms rapidity region, Δy, available for the first gluon emission (with transverse momentum $k_{\perp 1}$) is $\log(W^2/k_{\perp 1}^2)$ the two independent new dipoles may emit a gluon (with transverse momentum $k_{\perp 2} < k_{\perp 1}$) inside a total range

$$(\Delta y)_{gen} = \log(s_{12}/k_{\perp 2}^2) + \log(s_{23}/k_{\perp 2}^2) = \log(W^2/k_{\perp 2}^2) + \log(k_{\perp 1}^2/k_{\perp 2}^2) \qquad (16)$$

In the last expression we have used the lines after eq (10) and eq (11). Consequently there will by the emission be an increase in the allowed phase space, $\delta\lambda = \log(k_{\perp}^2)$. This can be conveniently "added" to the triangular phase space in fig 2a by extending a (double) fold as in fig 2b. Actually we are in this way adding a triangular region, made up of the two sides of the fold, to the original triangle. It is easy to see that each new emission has the same effect on phase space.

After several emissions we obtain a complex figure with many folds "sticking out" as in fig 2c. The length of the baseline, called λ, is given by the expression

$$\lambda \equiv \sum \log(s_{i,i+1}) = \log(s) + \sum \log(k_{\perp i}^2) \tag{17}$$

It can be interpreted as an effective rapidity range for the final produced hadrons and is strongly correlated to the hadron multiplicity, [16, 17]. The baseline is irregular and behaves like a (multi)fractal with the so-called anomalous dimension of QCD basically equal to the fractal dimensions, [18, 19].

3.2 The Webber-Marchesini Cascades

The Webber-Marchesini Cascade Model [20], which is described by the Monte Carlo simulation program HERWIG [21], is a conceptually very differnt approach to the multiple gluon emissions. A fundamental property is the angular ordering of the emissions in the cascade, which is a consequence of soft gluon interference, [22]. The results are nevertheless very similar to the ones obtained from the Dipole Cascade Model. The basic reason for this similarity is that *the building of dipoles in the cascade is actually the same as the requirement of angular ordering in the emissions* [7]. The two different cascades developing along different lines nevertheless cover the same phase space region of fig 2c. In the dipole scheme it is searched from top to bottom, while in the Webber-Marchesini scheme it is searched sideways going from a central angle or rapidity out towards the ends.

In order to see this we note that Webber-Marchesini use one angular variable, θ, and one energy variable, E. Remembering the relationship between the rapidity of a massless particle ("pseudo-rapidity" for all others):

$$y = \frac{1}{2}\log\left(\frac{e+p_l}{e-p_l}\right) = -\log\tan(\theta/2)) \simeq -\log(\theta/2) \tag{18}$$

and the approximate relation $k_\perp \simeq E\theta$ we may map these variables onto the quantities $(y, k_\perp)$ and consider the emission of a Webber-Marchesini cascade in the triangular phase space. The angular ordering means that after emitting a "first" gluon along a parton line (emission angle θ) the next emission must have an emission angle smaller than θ and so on. This means that in this kind of cascade you may start with a first emission at some angle or rapidity and then afterwards go towards the q-end in rapidity (ie following the emissions along the q-line) and afterwards go towards the $\bar{q}$-end in rapidity (ie following along the $\bar{q}$-line).

In both cases the "new" emissions are evidently fulfilling the angular ordering requirement (ie diminishing angles along the parton line). In every "step" in rapidity one searches through the possible $k_\perp$- (or E-)values, ie one "goes from one side in rapidity, y, towards the other, all the time looking up and down in $k_\perp$". Every time one finds an emission a "new" parton line starts out and *this corresponds exactly to adding a folded triangle* in the Lund language. Then they are searched through in the same manner, producing subfold triangles etc.

According to our description above, one is in the Lund DCM "going down in $k_\perp$ all the time looking left and right inside the relevant rapidity region", also adding folds and resolving them for new emissions. If all the gluons were *strongly* ordered the two schemes would give the same result, but in reality recoils and other nonleading effects cause some differences. Here perturbative QCD does not give a clear answer because in these regions interference effects are important and the probabilistic cascade does not give an exact description.

To give a complete description of an event, the parton cascade must be complemented with a hadronization model. In the end of the cascade Bryan Webber has introduced a "cluster" fragmentation scheme. In this way he builds chains of decaying clusters along the same regions where the Lund String is spanned and breaks up.

3.3 Sudakov Formfactors

We will next describe the probabilities for the occurrence of the different exclusive states in a partonic cascade. In a field theoretical treatment it is necessary to take into account the virtual corrections to the real emissions, which define the state. It is in general possible to sum up the large parts of the corrections to all orders (at least for a constant coupling) in most field theories. The result is then in general an exponential integral, called a Sudakov formfactor.

We can formulate the resulting probability for a bremsstrahlung emission together with the accompanying virtual corrections in the language of general probability theory. It is the probability to obtain just those gluon emissions which caracterize the state and nothing else. Assume that there is an *inclusive* probability dP_A to emit the specified set (denoted A) of gluons and that there should be no gluons emitted in the phase space region Ω, inside which there is an inclusive probability density dp. The probability for the *exclusive* probability is then given by the expression

$$dP_A \cdot \exp(-\int_\Omega dp) \tag{19}$$

A similar result is obtained for *semi-inclusive* cross sections, which is used in the cascades described above. Thus eg the probability that the *hardest* gluon (defined as the one with the largest $k_\perp$) is emitted with momentum specified by y_1 and $\vec{k}_{\perp 1}$, is given by the expression

$$dp(y_1, \vec{k}_{\perp 1}) \cdot \exp(-\int_{\hat{\Omega}} dp) \tag{20}$$

where $\hat{\Omega}$ is the phase space region with $k_\perp > k_{\perp 1}$, inside which no emission is allowed. A similar formfactor is obtained for the next hardest etc. In the Marchesini-Webber cascade, where the emissions are ordered in angle, the integration regions in the formfactors are in the same way bounded by the appropriate angles.

Quite generally, if no emission is allowed inside a limited phase space region $\hat{\Omega}$, but any emission is admitted inside its complement, then the appropriate Sudakov formfactor is given by

$$S = \exp(-\int_{\hat{\Omega}} dp) \tag{21}$$

4 Deep Inelastic Scattering Events

There is a major difference between the calculation of the cross sections for the DIS events and for the e^+e^--events, which we have treated in the previous section. As discussed above, the total cross section for e^+e^--annihilation is described by the lowest order (0:th order in α_s) diagram with small corrections of order α_s. This is not the case in DIS, where several fan diagrams, as in fig 1 give contributions in leading logarithmic order. For large Q^2 (the DGLAP region) the dominating contributions come from fan diagrams where the emitted gluons are strongly ordered in x (or $q_+ = q_0 + q_L$) and $q_\perp$. The contribution to the structure function from such a fan diagram is given by (cf eq (3))

$$\prod_i \bar{\alpha} \frac{dz_i}{z_i} \cdot \frac{dq_{\perp i}^2}{q_{\perp i}^2} \tag{22}$$

The fan diagram in fig 1 does not represent an exclusive final state. Such a state contains additional gluons emitted as final state radiation. The allowed phase space regions are specified by angular ordering constraints due to soft gluon coherence. The final state emission can be described in the same way as in e^+e^--annihilation, ie with specified probabilities for the emitted gluons and appropriate Sudakov formfactors. Thus a fan diagram as in fig 1 represents a *class of final states* with an arbitrary number of additional gluons in the regions allowed for final state radiation. Different states in a class will contain a common "essential" set of partons emitted, usually called "the initial state radiation".

We note that the fan diagram in fig 1 should not be directly interpreted as a Feynman diagram. The contribution from a specific Feynman diagram is neither gauge independent nor Lorentz covariant by itself. Thus eg the contributions in fig 4 depend on the gauge chosen, and interfere constructively and/or destructively in different parts of phase space to give the welldefined cross section. It may seem natural to describe the two contributions as initial and final state radiation respectively, but we conclude that the separation between initial and final state radiation is not unique, and cannot be based on Feynman diagrams.

Thus this separation has to be determined by specifying the boundaries in the phase space. If we interprete a particular fan diagram , as in fig 1, as the initial state radiation, its contribution to the structure function depends upon within which phase space region we allow final state emission. In the DGLAP approach the gluons in the fan diagram (the initial state emission) are ordered both in x and $q_\perp$, and final state emission is allowed within the regions determined by the angular ordering and energy conservation constraints.

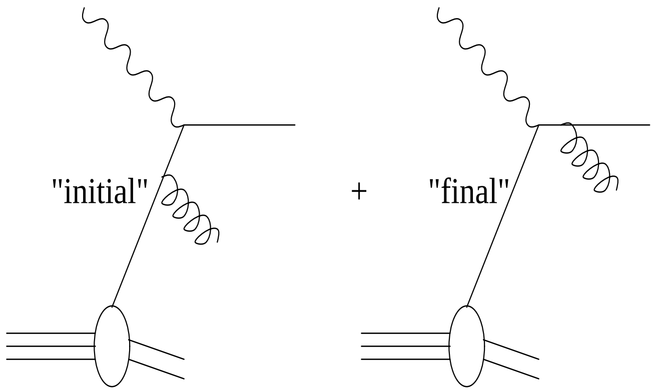

Figure 4: *"Initial" and "final" state radiation diagrams.*

We could choose to include more final state gluons in the initial state radiation. In that case we would have obtained contributions from more fan diagrams (more classes of final states), but in each case with a more restricted region for final state emission. To get the same final result, the contribution from each fan diagram would then not be of the form in eq (22), but would be suppressed by an appropriate Sudakov formfactor. This formfactor is determined by the region in which final state emission should not be allowed, although it is not kinematically forbidden.

Although the separation between initial and final state radiation can be chosen in different ways, it cannot be quite arbitrary. One necessary consistency requirement is of course that what is regarded as final state emission can be emitted from the gluons in the "essential initial set" with small or negligible recoils. We also assume that the gluons are color connected along the fan diagram.

In this section we will firstly review the results of Ciafaloni and Catani et al, [5, 6], and the way they have defined the essential set of emissions. We will refer to their method as the CCFM Model and we formulate their results in a language suitable for a treatment in terms of the triangular phase space we have used for dipole emission. Introducing a different separation between initial and final state emission, we will show that, after some simplification and modifications, the results of their work is the occurrence of a linked chain of primary dipoles. In this way we will be able to define the intial state radiation as the radiation necessary to obtain the precise dipole chain and the final state radiation is then the result of the emissions from these dipoles. We end by presenting the probabilities in this the Linked Dipole Chain (LDC) Model.

4.1 The CCFM (Catani-Ciafaloni-Fiorani-Marchesini) Model

Following ref [6] we first study a situation with only gluons, and postpone a discussion of the effects from the quarks to section 5. The last gluon in the chain is assumed to interact with a color neutral probe. The probe and the target ends will also be considered in more detail in the next section.

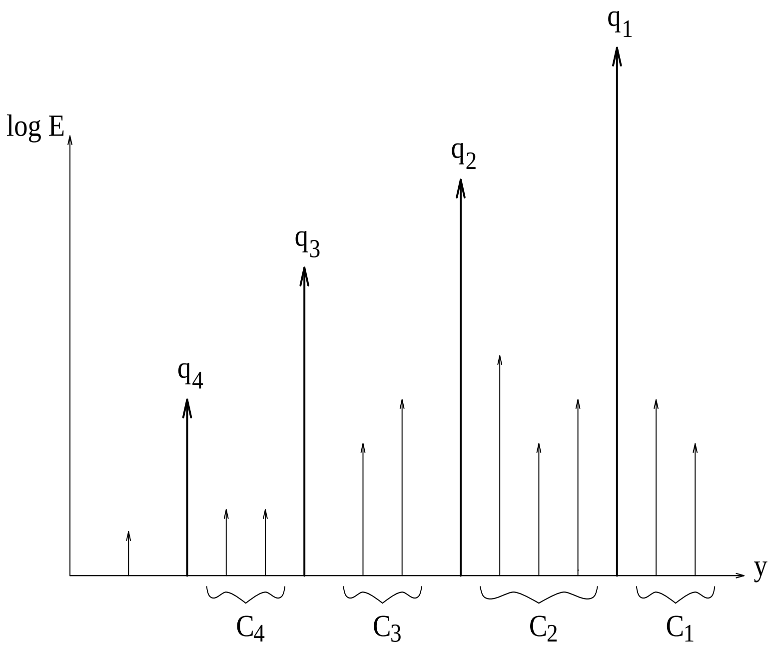

Figure 5: *An exclusive final state.*

Consider an exclusive final state with a large set of produced gluons as indicated in fig 5, where the gluons are ordered in rapidity (ie in angle). Select those gluons which are *not* followed in rapidity by a gluon with more energy (or lightcone momentum $q_+ = q_0 + q_L$). The gluons in this subset are called $q_1, q_2, ...$, see fig 5, and in the CCFM approach these gluons are the ones which are treated as initial state radiation, while the remaining gluons are treated as final state emission. (The group denoted C_1 can be regarded as emitted by the gluon q_1 with small recoils, etc). The state in fig 5 is thus one member of a class specified by the gluons q_i, which are ordered *both* in angle *and* in energy. This class thus contains all exclusive states with any possible final state emissions C_i.

The angular ordering of the gluons q_i in the fan diagram implies that they are also color ordered and there is a corresponding fan diagram as the one in fig 1. Since the gluons carry both color and anticolor, the color ordering means that the gluons are color connected when we go around the chain as indicated in fig 6.

Since the final state emission gluons in the group C_i are soft compared to the gluon q_i, this gluon can be regarded as on-shell and massless. The "connectors" with momenta k_i (cf fig 1) are however virtual and all spacelike. At every "vertex" there is energy momentum conservation so that

$$k_i = P - \sum_{m=1}^{i} q_m \quad \text{ie} \quad k_i = k_{i-i} - q_i \tag{23}$$

As in section 2 we introduce the variables z_i such that $k_{+i} = z_i k_{+(i-1)}$ and $q_{+i} = (1 - z_i)k_{+(i-1)}$ (and thus $k_{+i} = (\prod_{m=1}^{i} z_m) \cdot P_+$). The results of the CCFM model presented in ref [6] are obtained in the leading log approximation. At small values of x, the leading contribution corresponds to strong ordering in energy ($q_{+i} \ll q_{+(i-1)}$) which

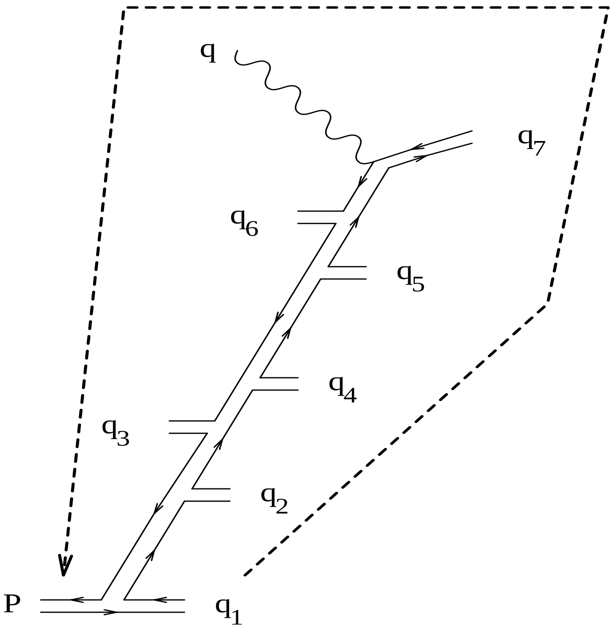

Figure 6: *The color flow in a DIS fan diagram.*

corresponds to z-values that are very small. In this case the the splitting functions $P(z)$ are dominated by the pole contribution $\propto 1/z$ and $q_{+i} = (1 - z_i)k_{+(i-1)} \approx k_{+(i-1)}$.

We can picture the gluon chain in a $(y, \log(k_\perp^2))$ plot similar to the one in fig 2 for e^+e^--annihilation. An example of this is shown in fig 7. For the on-shell momenta q_i, denoted by circles in fig 7, a point in this diagram also directly determines the value of $q_+ = q_\perp \exp(y)$. Thus $\log(q_+) = \frac{1}{2}\log(q_\perp^2) + y$ is increasing towards the upper righthand corner ($\log(q_-)$ increases in a symmetric way towards the upper lefthand corner). For the off-shell momenta k_i, for which the rapidity becomes imaginary, the crosses in fig 7 correspond to the values of $k_\perp$ and k_+.

In the leading log approximation, we may partition all the emission steps ($k_{i-1} \to k_i + q_i$) into the three different types:

1. $\vec{k}_{\perp i} \simeq -\vec{q}_{\perp i} \gg \vec{k}_{\perp(i-1)}$ (as an example cf the emissions denoted 1 and 2 in fig 7)
2. $\vec{k}_{\perp i} \simeq \vec{k}_{\perp(i-1)} \gg \vec{q}_{\perp i}$ (example, cf the emission denoted 3 in fig 7)
3. $\vec{q}_{\perp i} \simeq \vec{k}_{\perp(i-1)} \gg \vec{k}_{\perp i}$ (example, cf the emission denoted 4 in fig 7)

The angular ordering implies that eg q_3 lies to the left of the dashed line through q_2. We also note that according to ref [6] only contributions satisfying the kinematical constraint

$$k_{\perp i}^2 > z_i q_{\perp i}^2 \tag{24}$$

should be included in the essential emission set. This means in particular that k_4 must lie above the dotted line through q_4 in fig 7. Contributions from emissions violating this

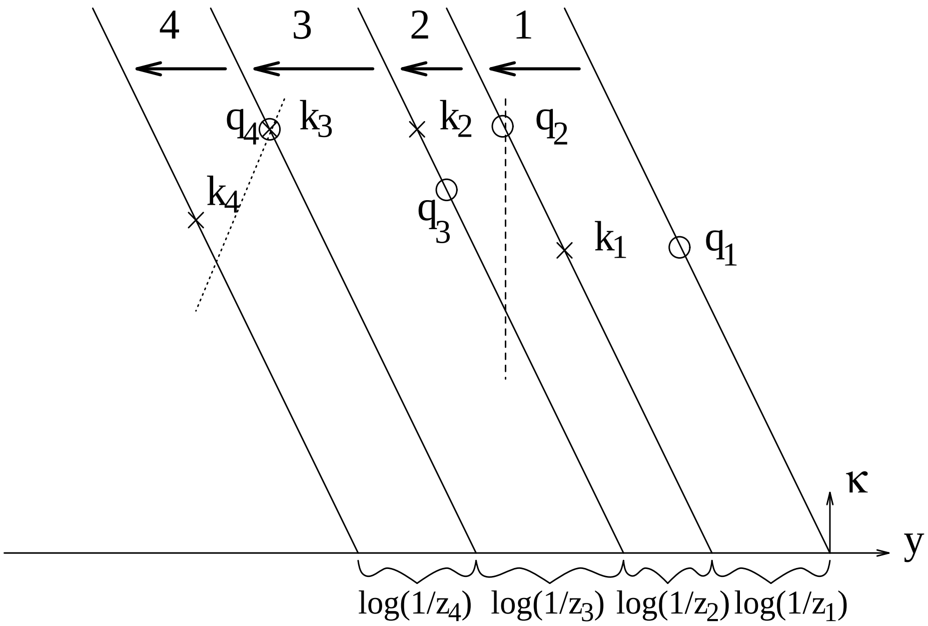

Figure 7: *The different type of steps in a gluon chain in a $(y, \log(k_\perp^2))$ plot. The circles mark the produced real gluons q_i and the crosses mark the virtual connectors k_i.*

constraint are suppressed because they would correspond to situations where $|k^2| \gg k_\perp^2$. This constraint will be essential for our results in the following.

Each step in the emission chain is in the CCFM Model described in terms of the weight

$$\bar{\alpha}\frac{dz_i}{z_i}\frac{d^2 q_{\perp i}}{\pi \vec{q}_{\perp i}^{\,2}}\Delta_{ne}(z_i, k_{\perp i}, q_{\perp i}) \tag{25}$$

with the so-called non-eikonal formfactor $\Delta_{ne}(z_i, k_{\perp i}, q_{\perp i})$ given by the expression

$$\Delta_{ne}(z, k_\perp, q_\perp) = \exp\left[-\bar{\alpha}\log(1/z)\log\left(\frac{k_\perp^2}{zq_\perp^2}\right)\right] \equiv \exp(-\bar{\alpha}A) \tag{26}$$

As we will demonstrate, this is an expression of the Sudakov kind. It can be interpreted as the negative exponent of an integrated emission probability over the region in which further emission is not allowed. This area is denoted A in eq (26) and in fig 8, which shows the situation in the three different types of steps mentioned above.

The expression in eq (26) is obtained as a result of contributions from real and virtual emissions with momenta p in the region $k_+ < p_+ < q_+$ bounded by the lines l_1 and l_2 in fig 8. Real emissions give a contribution in the angular (rapidity) ordered region to the left of the line l_3. The region B to the right of the line l_3 corresponds to emissions which are not angular ordered. As mentioned above, such emissions are included in the final state radiation, and therefore they give no contribution to the formfactor. In the region C above the line l_4, virtual corrections give a contribution which exactly cancels that from the real emissions, thus leaving only the area A. Fig 8a and fig 8b illustrate case 1 and 2 respectively. For case 3 the region D is also excluded, as shown in fig 8c. This is related to the constraint $k_\perp^2 > zq_\perp^2$, which implies that no real emissions are allowed in this region.

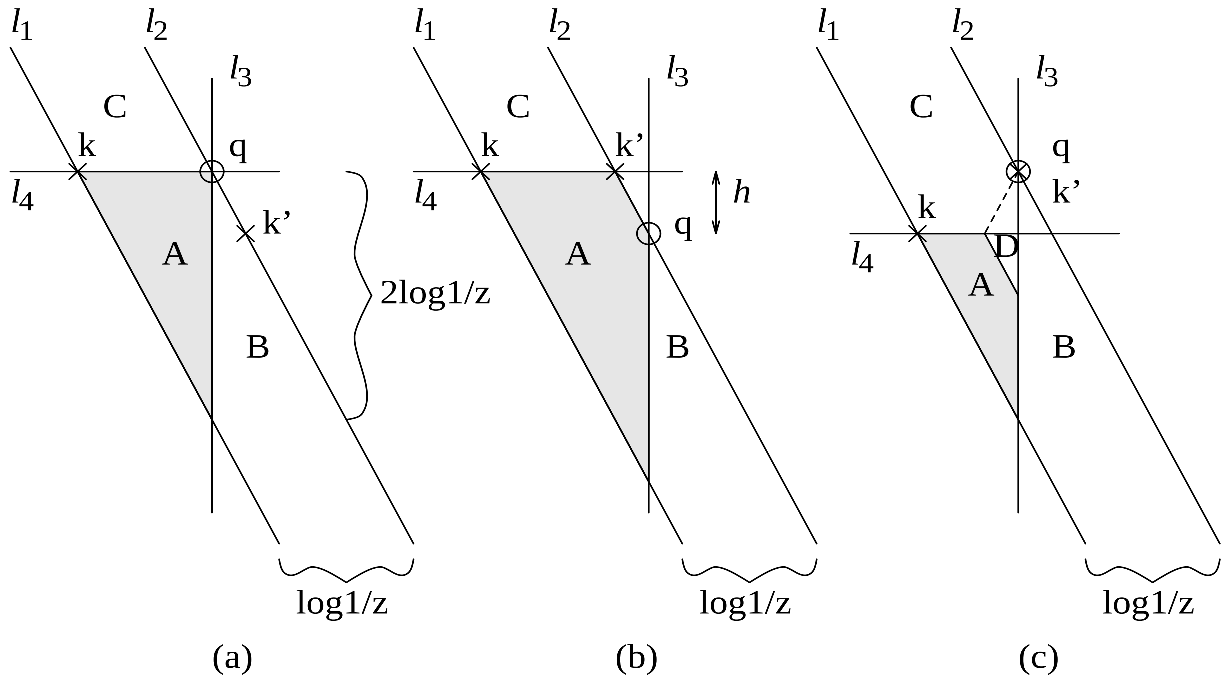

Figure 8: *The relevant areas, in the leading log approximation, for the three different types of steps in the gluon chain. (a): $k_\perp \approx q_\perp \gg k'_\perp$, (b): $k_\perp \approx k'_\perp \gg q_\perp$, (c): $q_\perp \approx k'_\perp \gg k_\perp$. The distance h in (b) is given by $h = \log(k_\perp^2/q_\perp^2)$*

We end by the remark that all the on-shell q-emission vectors are in this pictorial formalism described as extended folded triangles in the same way as we described them in the DCM. Emissions in these folds (cf fig 2) correspond to final state emissions in addition to those in the B-regions in fig 8.

4.2 Reformulation and Analysis, The Linked Dipole Chain Model

As mentioned above, the formfactor Δ_{ne} does not get any contribution from gluons in area B in fig 8, because such gluons are treated as final state emission and inclusively summed over. Consider the situation in fig 9. The gluon marked $\hat{q}$ is such a gluon. In fig 5 it would belong to the group C_1 and it can be regarded as final state emission from the quasireal gluon q_2, since it has smaller values for all momentum components $q_\perp$, q_+ and q_-. (Note that q_+ and q_- grow symmetrically towards the upper right and upper left corners as indicated in fig 9.) In the leading log approximation all momenta are strongly ordered, which means that the virtual mass and the recoil experienced by gluon q_2 are negligibly small.

The same arguments can however be used to also treat the gluon q_3 in fig 9 as final state emission from gluon q_2. (The inequality $q_{-3} < q_{-2}$ is satisfied if q_3 lies to the right of of the dotted line in fig 9.) Thus the two steps in fig 10a are replaced by a single step as in fig 10b. (Remember that these diagrams should not be interpreted as Feynman diagrams.) Since q_3 is softer we have $q_{23} = q_2 + q_3 \approx q_2$ and q_{23} takes the same position as q_2 in the diagram in fig 9. The z-value for this single step is given by the relation $k_{+3} = z_{23} \cdot k_{+1}$, which implies $z_{23} = z_2 \cdot z_3$.

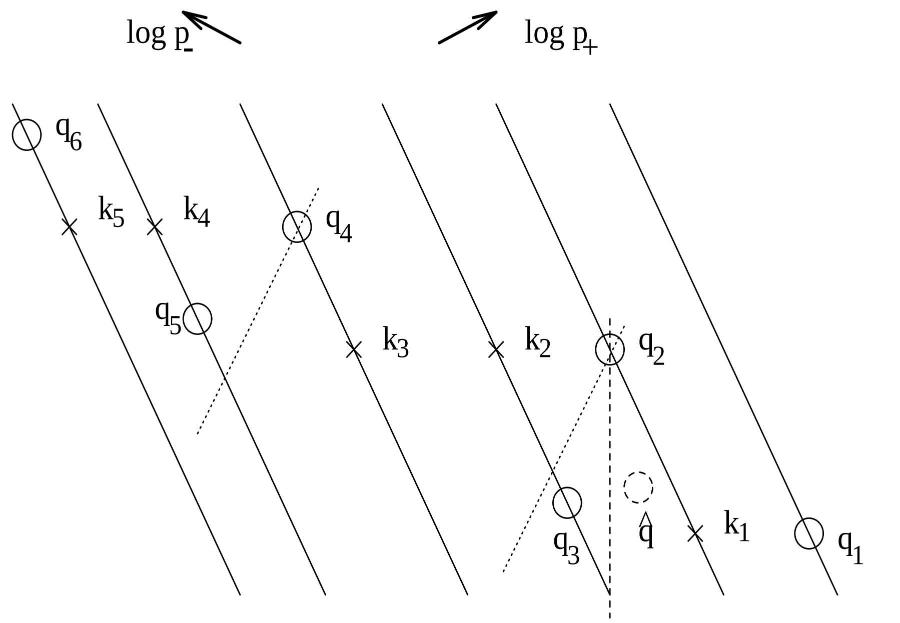

Figure 9: *Including more gluons in the final state radiation.*

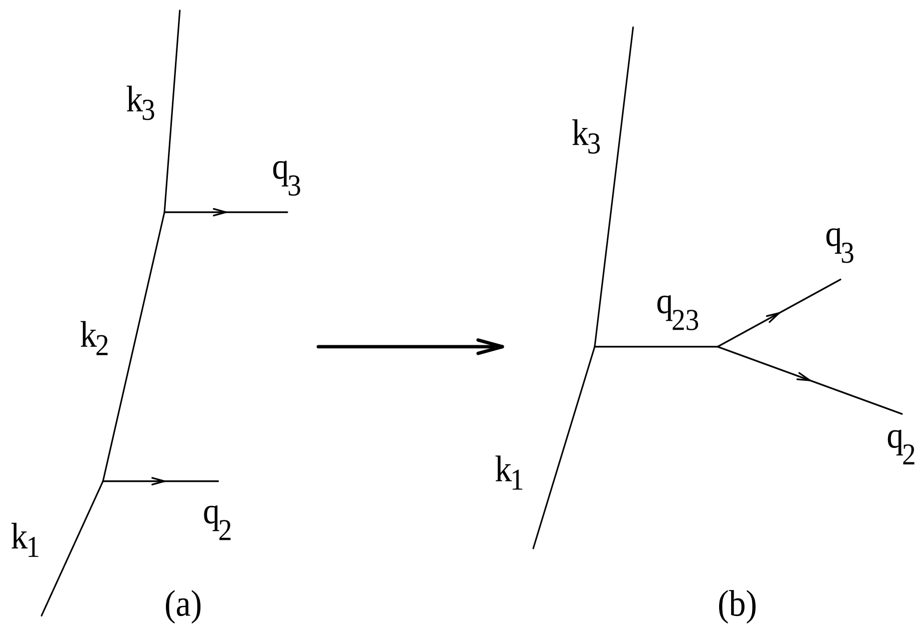

Figure 10: *Two initial state emissions as in (a) can be replaced by a single step as in (b).*

In the dipole formalism it is actually possible to include even more gluons in the final state emission. This is so, because in the dipole formalism softer gluons are emitted by the *separation* of a color charge and anticharge located in two different parent gluons, which thus share the recoil. An example is shown in fig 9, where the gluon q_5 can be regarded as final state emission from the dipole between q_4 and q_6. Thus q_4 can take up the positive lightcone component of the recoil, q_{+5}, while q_6 takes up the negative component, q_{-5}. In this way the recoils to both q_4 and q_6 become small.

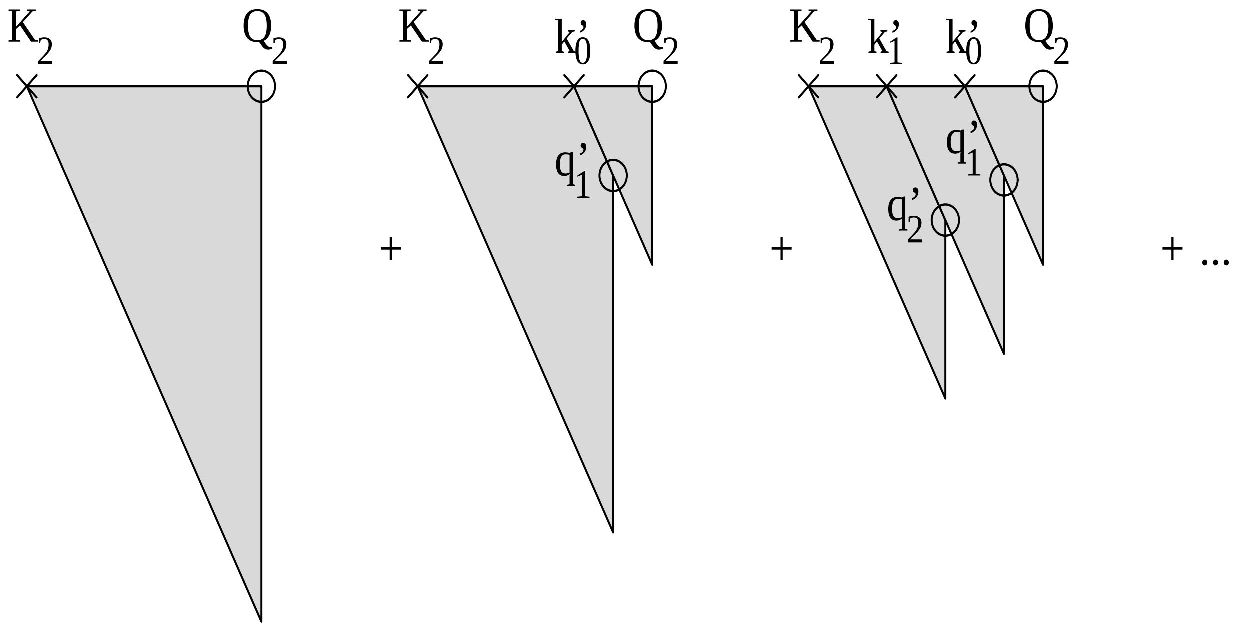

Figure 11: *Summing up the contributions from intermediate steps.*

The net result is that *all* gluons q_i in the initial chain, which satisfy the constraint $q_{\perp i} < \min(q_{\perp(i-1)}, q_{\perp(i+1)})$ (and of course the angular ordering constraint $y_{i+1} < y_i < y_{i-1}$), can be absorbed into the final state emission, provided that for a specified fan diagram, the phase space for final state emission is correspondingly increased. This implies that all steps of type 2 ($k_{\perp i} \approx k_{\perp(i-1)} \gg q_{\perp i}$) disappear and become absorbed into steps of type 1 or type 3. Thus we are left with a set of "primary" gluons Q_i, which are connected in a fan diagram only via steps of these two types, ie via steps where the tranverse momenta of the connectors K_i (satisfying $Q_i + K_i = K_{i-1}$) are either increasing or decreasing. In both cases we find that

$$Q_{\perp i} \approx \max(K_{\perp(i-1)}, K_{\perp i}) \tag{27}$$

Thus in our formalism, a single fan diagram specified by the gluons Q_i, corresponds to several different fan diagrams in the CCFM formalism. To obtain the contribution to the structure function from this single diagram in our formalism, we therefore have to sum up all the different contribution in the CCFM formalism. Consider a step of type 1 with momenta Q_2 and K_2 as shown in fig 11. In the CCFM formalism this gets contributions from fan diagrams with $0, 1, 2, ...$ gluons q'_l in between. Each contribution contains a product of formfactors $\exp(-\bar{\alpha}A_l)$ (cf fig 8). This product is thus given by $\exp(-\bar{\alpha}A)$, where A is the total area of the shaded regions in fig 11). If we sum over the number of intermediate gluons q'_l and integrate over their momenta (within the allowed regions) it is not difficult to realize that the form factor is exactly compensated.

$$\sum_n \prod_l^n \int \bar{\alpha} \frac{dz'_l}{z'_l} \frac{d^2 q'_{\perp l}}{\pi {q'_{\perp l}}^2} \Delta_{ne} = 1 \tag{28}$$

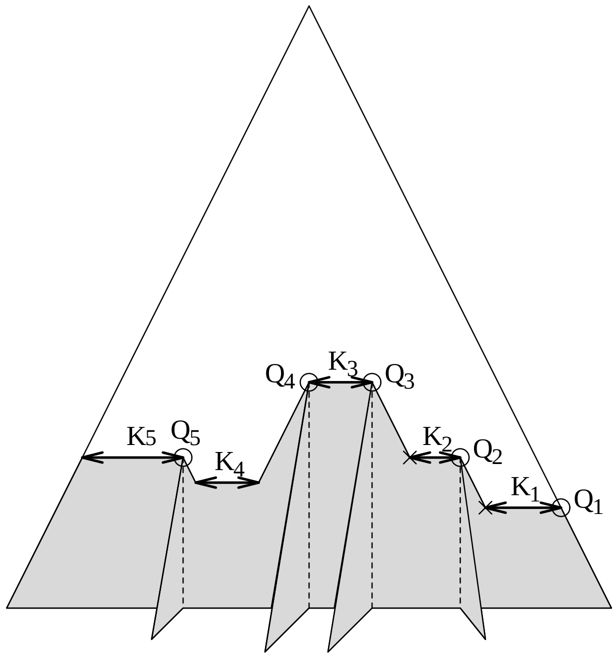

Figure 12: *A gluon chain in the LDC model. The endpoints of the arrows which mark the connectors K_i, represent the points $(K_{\perp i}, K_{+i})$ and $(K_{\perp i}, -K_{-i})$ respectively (see the text).*

(For a formal proof, see the appendix.) Thus the net result is a total weight

$$\bar{\alpha}\frac{dz_i}{z_i}\frac{d^2Q_{\perp i}}{\pi Q_{\perp i}^2} \tag{29}$$

(Here of course $z_i = K_{+i}/K_{+(i-1)}$.) The same result is obtained if the step is of type 3, ie if $K_{\perp i} \ll Q_{\perp i} \approx K_{\perp (i-1)}$.

We are then left with a chain of steps up and down in transverse momentum according to the types 1 and 3. The associated emitted gluons Q_i form a chain of linked dipoles, which we call *primary dipoles*. Such a chain is illustrated in fig 12, and it represents a class of final states where final state radiation is allowed in the whole shaded region in fig 12. The contribution to the structure function, or to the cross section, from this chain, is a product of weight factors without any extra formfactors, similar to the product in the DGLAP evolution.

The allowed region for final state emission can be naturally interpreted. When eg the gluons Q_i and Q_{i+1} move apart, their color charges are separated and thus emit gluon bremsstrahlung. However, in the production chain, Q_i and Q_{i+1} are connected by a virtual gluon with momentum K_i. In a semiclassical picture they are therefore not produced in a well-defined single point, but there is some uncertainty in the localization determined by the virtuality of the connecting gluon. The current associated with the two emitted gluons starts out with a space time size, corresponding to a transverse distance, b_i, defined by the virtuality $b_i \simeq 1/\sqrt{-K_i^2} \simeq 1/K_{\perp i}$. It is very difficult to obtain radiation with a wavelength smaller than this available antenna size. Thus emission with transverse momentum larger

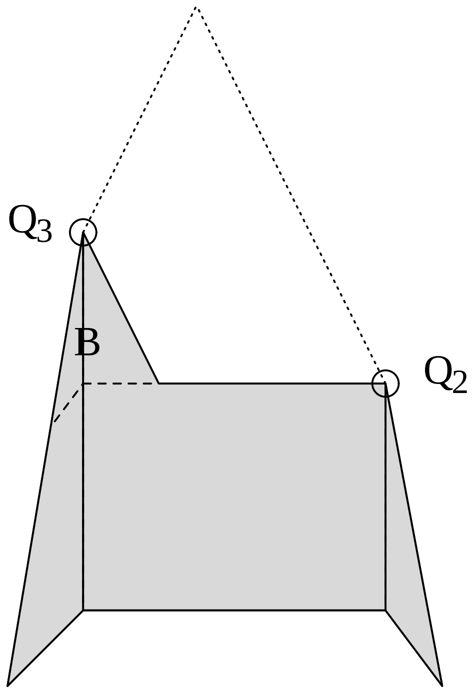

Figure 13: *The allowed phase for final state emission from a dipole in the chain of primary gluons.*

than $1/b_i \simeq K_{\perp i}$ is suppressed. This is related to the results of ref [6] that the non-eikonal formfactor does not get any contribution from the region C in fig 8. As mentioned above, in this region, which corresponds to transverse momenta larger than the virtuality $K_\perp$, *real and virtual contributions cancel each other.*

Looking at fig 12, the allowed region for final state emission in a primary dipole does not appear to be bounded by a fixed value for the transverse momentum. This is however actually the case in the *rest frame of the relevant dipoles.* Study eg the dipole stretched between the neighbouring gluons Q_2 and Q_3 in the chain in fig 12, which is also shown in fig 13. Final state emission is here allowed in the shadowed region. Consider the rest frame of the dipole where both Q_2 and Q_3 have vanishing transverse momenta and study gluon emission with $q_\perp < \sqrt{-K_2^2}$ in this frame. If we boost back to the initial Lorentz frame, specified by the probe and target directions, then the radiation will cover just the region indicated in fig 13. In particular, gluons which in the rest frame have large longitudinal momenta in the direction of Q_3, will cover the region indicated B in fig 13.

We also note that our formalism is explicitly left-right symmetric, ie symmetric if we study the chain from the probe end instead of the target end. This symmetry is not obvious in the CCFM formalism, and we will in the next section further exhibit this property. As mentioned above, gluons satisfying the relation $q_{-(i+1)} < q_{-i}$ are included in the final state emission. Therefore all gluons Q_i in the primary chain satisfy

$$Q_{-(i+1)} > Q_{-i} \tag{30}$$

Thus the produced gluons are ordered both in Q_+ and Q_-. We can consider the same chain as before, but this time analyse the results from the probe end and study the steps $L_i \equiv -K_i \to Q_i + (-K_{i-1}) \equiv Q_i + L_{i-1}$ using the variables z_- defined by $K_{-i} = z_{-i}K_{-(i+1)}$ (or $L_{-i} = z_{-i}L_{-(i+1)}$). In the leading log approximation we have $L_{-i} = -K_{-i} \approx Q_{-i}$. We remember that in our phase space diagram $\log p_+$ and $\log p_-$ increase symmetrically towards the upper right and upper left corners respectively. Therefore the connectors K_i can be represented by two points corresponding to $(K_{\perp i}, K_{+i})$ and $(K_{\perp i}, -K_{-i})$, which are connected by arrows in fig 12. The gluon Q_i is emitted "between" K_{i-1} and K_i, and thus we have in every step $Q_{+i} \approx K_{+(i-1)}$, $Q_{-i} \approx -K_{-i}$ and $Q_{\perp i} \approx \max(K_{\perp(i-1)}, K_{\perp i})$.

Actually our two-dimensional description in the phase space triangle completely neglects the dependence on the azimuthal angles ϕ_i. An emitted on-shell gluon in the primary set is described by a single point, representing all values of $0 \leq \phi_i < 2\pi$ (but containing precise information of its $Q^2_{\perp i}$ as well as its lightcone components $Q_{\pm i}$ with $Q_{+i}Q_{-i} = Q^2_{\perp i}$). We note that this implies that the positions of the points Q_i in fig 12 are not enough to specify the chain, since the values $Q_{\perp i}$ do not specify $K_{\perp i} = |\sum^i \vec{Q}_{\perp l}|$. The length of $\vec{K}_{\perp i} = \vec{K}_{\perp(i-1)} - \vec{Q}_{\perp i}$ depends sensitively on the relative angles when $Q_{\perp i} \approx K_{\perp(i-1)}$. Within the leading log approximation the chain *is* however well specified by *either* the values $(K_{\perp i}, K_{+i})$ *or* $(K_{\perp i}, K_{-i})$. As example we show that all momenta can be reconstructed from the quantities $(K_{\perp i}, K_{+i})$. As mentioned above, we have $Q_{\perp i} \approx \max(K_{\perp(i-1)}, K_{\perp i})$, which follows from the fact that small $Q_\perp$ are not included in the primary set of gluons. Q_{+i} and Q_{-i} are determined from the relations $Q_{+i} \approx K_{+(i-1)}$ and $Q_{-i} = Q^2_{\perp i}/Q_{+i}$. Finally K_{-i} is fixed by the relation $-K_{-i} = Q_{-i}$.

For this reason we want to rewrite the weight in eq (29) in terms of K_i, using the relations $d^2K_{\perp i} = d^2Q_{\perp i}$, $z_i = K_{+i}/K_{+(i-1)}$ and $Q^2_{\perp i} \approx \max(K^2_{\perp(i-1)}, K^2_{\perp i})$. In this way we get the following weight for each step in the chain

$$\bar{\alpha}\frac{dz_i}{z_i}\frac{d^2K_{\perp i}}{\pi K^2_{\perp i}}\frac{K^2_{\perp i}}{\max(K^2_{\perp(i-1)}, K^2_{\perp i})} \tag{31}$$

We have in this way defined a model to be called the Linked Dipole Chain (LDC) Model by the requirements that the weights for all "steps" are defined by eq (29) or eq (31) and that the ensuing primary dipoles defined by two neighbouring vectors Q_i will emit radiation in their restframes up to the $p_\perp$-value defined by the virtual connector K_i in between them. In this way we can account for all the final state radiation as the possible radiation from the primary dipoles at the same time as we obtain a simple expression for the contribution to the structure function from each primary dipole chain. The last factor in (31) will make it difficult to "go down" in transverse momentum along the chain. The product over the weight factors (31), integrated over all chains (as they have been defined above with the requirement that $\prod_i z_i = x$) is then just as in eq (3) the structure function, ie the partonic flux.

Any maximum in transverse momentum along the chain, cf fig 12, will give two primary gluons Q_i and Q_{i-1} with large transverse momenta, $Q_{\perp i} \approx K_{\perp i} \approx Q_{\perp(i-1)}$. The product of the weight factors in eq (31) will then provide a combined factor $(Q_\perp^{-2})^2 \simeq K^{-4}$, which is just the contribution valid for a Rutherford scattering. We will discuss this feature further in the following section.

5 Generalizations

In this section we want to discuss some generalizations of the results in the CCFM model. This includes a treatment of subleading contributions (including quarks in the parton chain) and a unified treatment of "normal DIS", boson-gluon fusion events and hard resolved photon-proton scattering. We also give further comments on the symmetry of the process.

5.1 Subleading Contributions and the Chain Endpoints

The results for the CCFM model presented in ref [6] are obtained for purely gluonic fan diagrams in the leading log approximation. It would be desirable to go beyond this approximation and include nonsingular terms in the splitting function. Such subleading terms are not considered in connection with the definition of the non-eikonal formfactor, eq (26). A reasonable conjecture (to be investigated in future publications) is that, if these corrections are included, then there will be the same cancellation between the real and virtual contributions as described in the previous section and that the summation in eq (28) still adds up to unity. Therefore *we assume that the weight defined by eq (31) is still relevant if we include the nonsingular terms in the relevant splitting function $P(z)$ to define the dipole chain in the LDC Model.*

Nonleading contributions are also obtained by quark contributions in the fan diagram. The splitting function $P_{g\to q\bar{q}}$ is nonsingular and therefore the weight analogous to eq (31) is not $\propto d(\log(1/z))$, but on a logarithmic scale bounded to z-values of order 1. If the probe is a virtual photon, a Z or a W, it can however only interact with quarks and in the leading log approximation the last step in the chain has $\log(z) \approx 0$.

Quarks are important also in the target end of the chain. The initial parton in the perturbative chain, marked P in fig 1, is a parton in the initial target hadron at some low virtuality Q_0^2. It is described by a structure function $F(x, Q_0^2)$, and the total result is obtained from a convolution of the perturbative chain and this function $F(x, Q_0^2)$. We here get three different contributions, when the initial parton is a gluon, a quark or an antiquark. In the first case, the chain is color connected to the remainder of the target hadron, which is then a color octet, see fig 14a and fig 6. If the initial parton is a quark or an antiquark, it is via a loop as in fig 14b color connected to the target remainder, now being a color $\bar{3}$ or 3 respectively. The nonleading contributions and the connection to the initial proton will be further studied in future work.

5.2 Boson-gluon fusion and hard resolved photon-proton scattering

In analyses of the structure functions it is generally assumed, as it is in ref [6], that the dominating contributions come from chains where all the gluons have transverse momenta

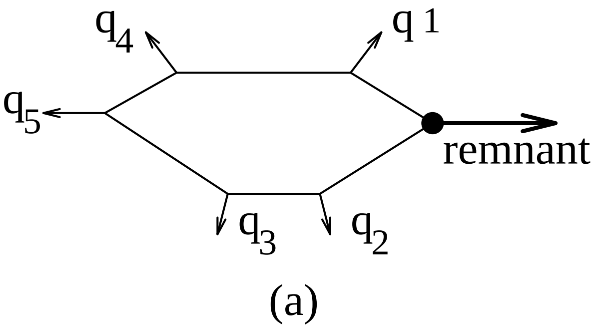

Figure 14: *The connection of color if (a): the initial parton is a gluon or (b): if the initial parton is a quark or an antiquark.*

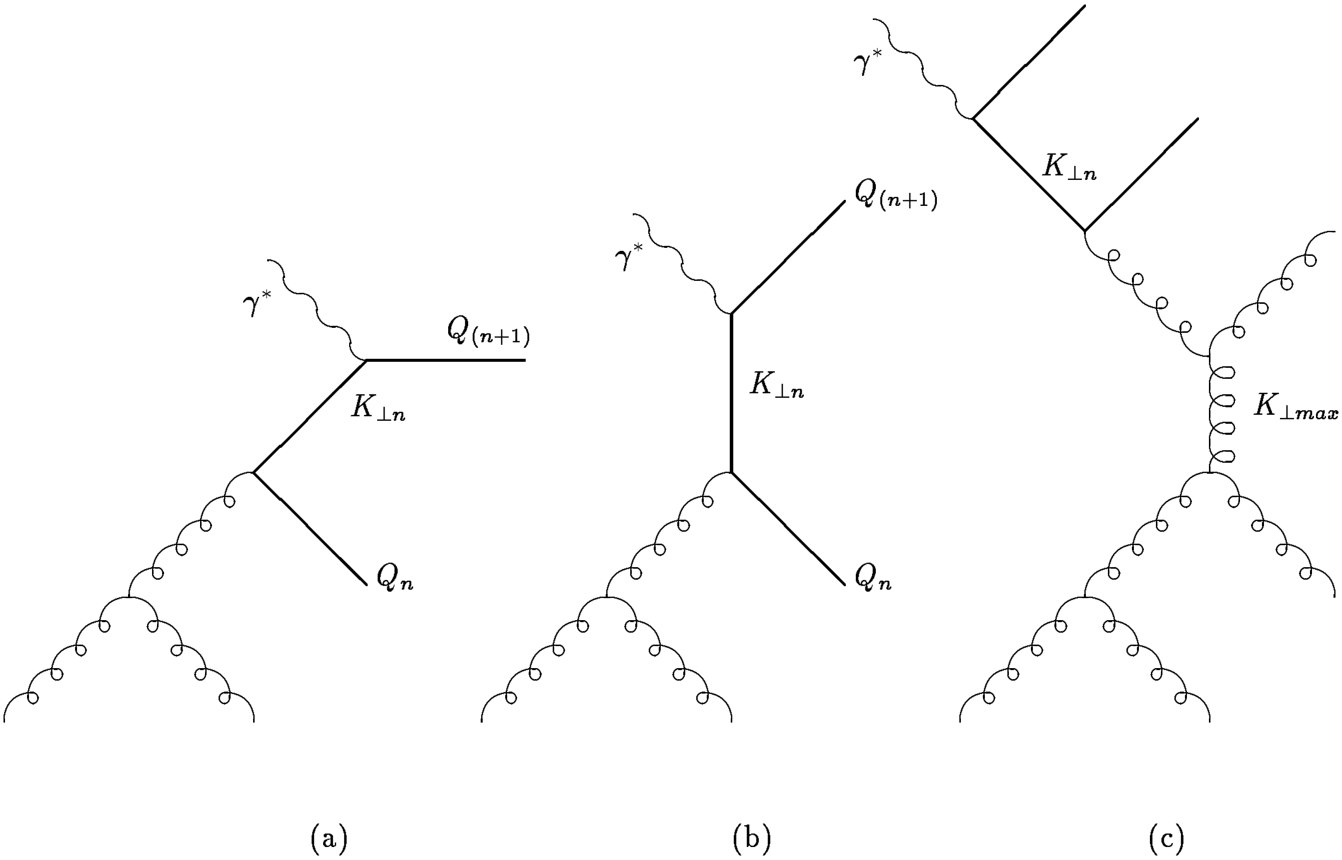

Figure 15: *Conventional pictures for (a) "normal DIS", where $Q^2 > K^2_{\perp n}$, (b) boson-gluon fusion where $K^2_{\perp n}$ is the largest virtuality in the event and (c) hard resolved photon-hadron scattering, where the largest virtuality, corresponding to a hard parton-parton scattering, is somewhere in the middle of the chain.*

smaller than $\log(Q^2)$ ("normal DIS", cf fig 15a). In our formalism it is easy to also include chains where one or more of the emitted gluons have larger transverse momenta. Although these contributions are suppressed they can be essential for smaller values of Q^2, or when one is interested in rare final states with high-$p_\perp$ jets.

The structure function is conventionally obtained by integrating over the transverse momentum for the *last* virtual gluon, $k^2_{\perp n}$, from $k^2_{\perp min} = \mu^2$ to Q^2. Introducing the "nonintegrated

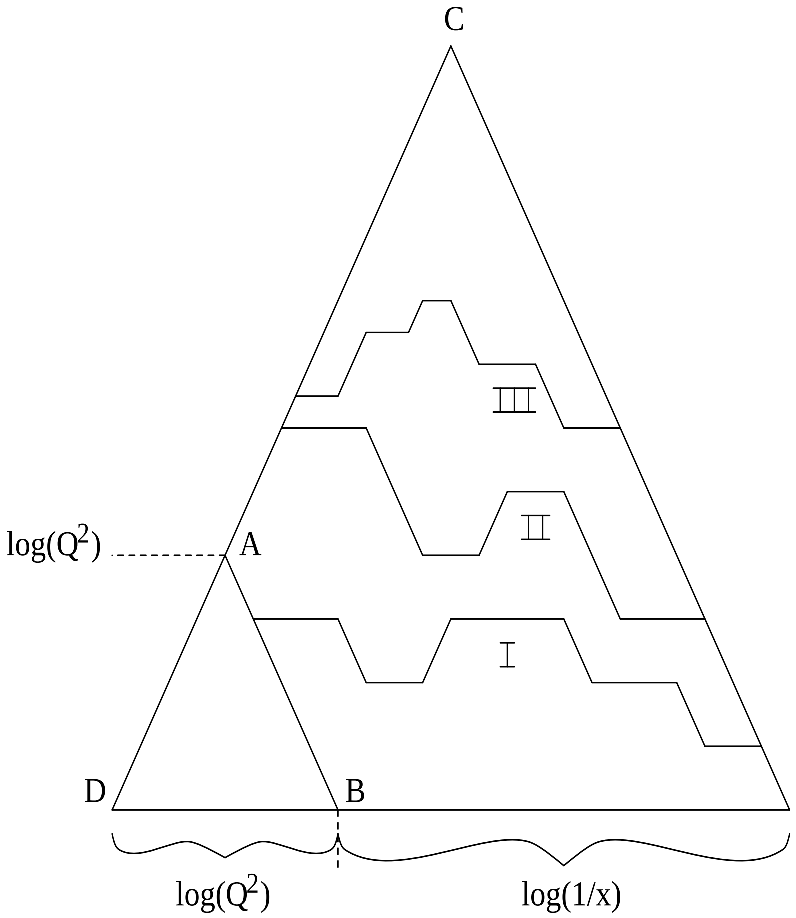

Figure 16: *Three different types of gluon chains.*

structure function" $\mathcal{F}(x, k_\perp^2)$ we then have

$$F(x, Q^2) = \int_{\mu^2}^{Q^2} \frac{dk_\perp^2}{k_\perp^2} \mathcal{F}(x, k_\perp^2) \tag{32}$$

where $x = \prod^n z_i$ is fixed equal to $x_{Bj} = Q^2/(2m\nu)$. Thus in the phase space triangle in fig 16 the chain should end somewhere on the line AB (see the chain marked I in fig 16). After absorption of the probe momentum we obtain a final gluon with momentum Q_{n+1}, which is located on the line CD in fig 16, which corresponds to $Q_- = P_{-probe}$. (Since the probe has no transverse momentum we have $Q_{\perp(n+1)} = K_{\perp n}$.)

If we also allow chains with $K_{\perp n}^2 > Q^2$, we note that such chains must have $K_{+n} = x_n \cdot P_+$ with $x_n = \prod^n z_i \neq x_{Bj}$. The "last" produced gluon (see fig 15) has $Q_{\perp(n+1)} = K_{\perp n}$ and $Q_{-(n+1)} \approx P_{-probe}$, where P_{probe} is the momentum of the probe. This implies

$$K_{+n} = -P_{+probe} + Q_{+(n+1)} = \frac{Q^2}{P_{-probe}} + \frac{Q_{\perp(n+1)}^2}{Q_{-(n+1)}} \approx \frac{Q^2}{P_{-probe}} + \frac{K_{\perp n}^2}{P_{-probe}} \tag{33}$$

The first term is by definition equal to $x_{Bj}P_+$, but for $K_{\perp n}^2 > Q^2$ the second term dominates. In this case the chain ends somewhere on the line AC in fig 16, and we have $Q_{+(n+1)} \approx K_{+n}$.

If the last $K^2_{\perp n}$ is the largest in the chain, and if it is larger than Q^2, we have a situation as the one marked II in fig 16. This corresponds to a *photon-gluon fusion event*, ie a hard scattering (with $p_\perp^2 > Q^2$) between the photon and the gluon as in fig 15b. The largest vituality in the event is *not* the Q^2 of the photon probe, but the $K_\perp$ of the exchanged parton.

It is necessary to remember however, that, due to the kinematical factors in the definition of the structure function, the contributions from these chains to the structure function are also weighted with the factor

$$Q^2/K^2_\perp < 1 \tag{34}$$

This factor is analogous to the factors $K^2_{\perp i}/K^2_{\perp(i-1)}$ in eq (31), when we "go down" in $K_\perp$ along the chain. Thus these chains give small contributions to the structure function (ie to the total cross section), but they are essential when we study high-$p_\perp$ jets. We think that it is very valuable that they can be described together with the "normal" events in a unified treatment.

We can also have situations where the largest $K_\perp$ is in the middle of the chain, as the one marked III in fig 16. This situation corresponds to a hard scattering between a parton in a resolved photon and another parton in a target cascade, see fig 15c. We have a suppression when we "go down" in $K_\perp$ from $K_{\perp max} \equiv K_{\perp m}$ to $K_{\perp n}$. For the whole chain we get a product of factors $K^2_{\perp i}/K^2_{\perp(i-1)}$ (cf eq (31))

$$\frac{K^2_{\perp(m+1)}}{K^2_{\perp m}} \cdot \frac{K^2_{\perp(m+2)}}{K^2_{\perp m+1}} \cdot \ldots \cdot \frac{Q^2}{K^2_{\perp n}} = \frac{Q^2}{K^2_{\perp max}} \tag{35}$$

where the last factor in the product is a consequence of our definitions and is analogous to the expression in eq (34).

We note that this result corresponds exactly to what we expect for a hard resolved photon-proton scattering. There are two cascades originating from the photon and the proton respectively, with a factor $dK^2_\perp/K^2_\perp$ for each branching, together with a factor $dK^2_{\perp max}/K^4_{\perp max}$ from the hard scattering between the last partons in the two cascades. The last factor obviously corresponds to such a hard Rutherford parton-parton scattering.

We note that the correct result is obtained also when the hard scattering corresponds to quark exchange, if the singular term $1/z$ from P_{gg} is canceled to account for the nonsingular behaviour of P_{qg}. The Mandelstam variables $\hat{s}$ and $\hat{t}$ for the hard subprocess are related to the variables $K^2_{\perp m}$ and z_m by the equations

$$-\hat{t} \approx K^2_{\perp m} \quad , \quad \hat{s} \approx Q_{+m} Q_{-(m+1)} \approx K^2_{\perp m}/z_m \tag{36}$$

Thus the squared matrix elements for gluon exchange ($\sim 1/\hat{t}^2$) and quark exchange ($\sim 1/\hat{s}\hat{t}$) differ just by a factor z_m.

We also want to stress the symmetry between the photon end and the proton end, and the fact that it is always the largest $K_\perp$ which has the fourth power of $K_\perp$ in the denominator, and is interpreted as the hard scattering. Of course we can also have more than one local

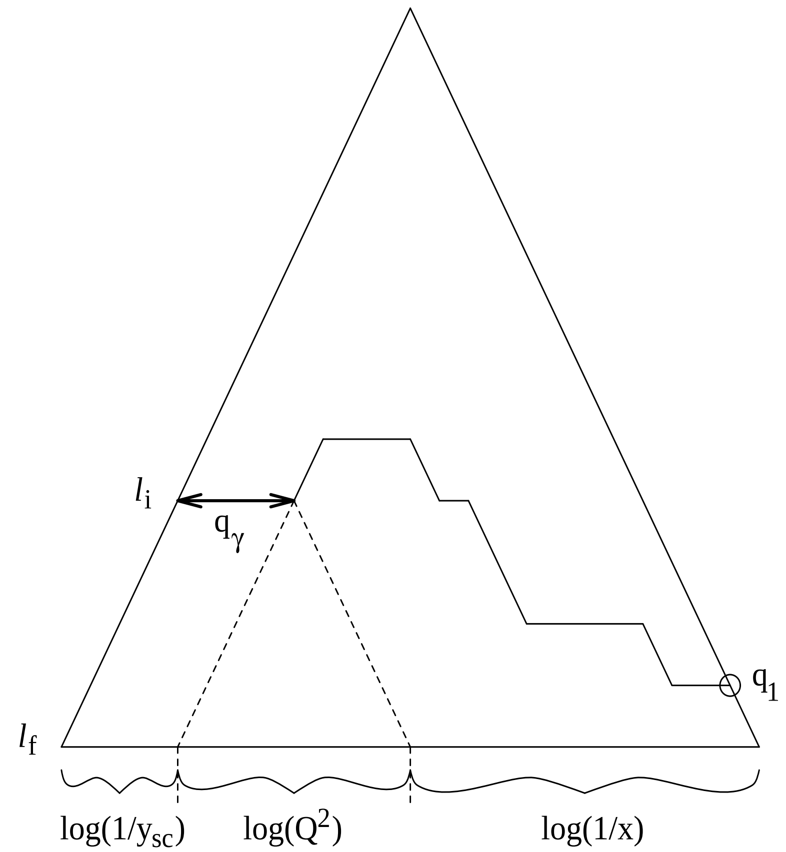

Figure 17: *The phase space situation if the recoiling electron is included.* y_{sc} *is the conventional scaling variable,* $y_{sc} = \nu/E$*, and not the rapidity.*

$K_\perp$ maximum in the chain, in which case we get extra suppression factors which become stronger when the valley in between the maxima becomes deeper.

Naturally, these results are also applicable to real photon-proton scattering and high-$p_\perp$ scattering in hh or $\gamma\gamma$ collisions. We note in particular that the $p_\perp$ in the initial state radiation is always bounded by the transverse momentum in the hard Rutherford scattering. This result was previously pointed out in ref [23].

5.3 Including the scattered lepton

It is also very interesting to study the total event including the initial and the scattered electron (see fig 1). The photon behaves here in the same way as the exchanged gluons in the chain. If we go to the rest frame of the initial electron (with momentum l_i) and the proton, and measure transverse momenta orthogonal to this axis, we find that in leading approximation the transverse momenta of the gluons are essentially unchanged, while the virtual photon and the recoiling electron (with momentum l_f) both get transverse momenta determined by $l^2_{\perp f} = q^2_{\perp\gamma} \approx Q^2$. In this frame the chain looks as in fig 17, which clearly illustrates the equivalence between the photon and the exchanged gluons.

Finally we note that the structure function F is defined such that

$$\frac{d\sigma}{d\log(x)d\log(y_{sc})} \sim \frac{1}{Q^4}\cdot F \tag{37}$$

where y_{sc} is the conventional scaling variable ν/E_i and not the rapidity. Since F contains the extra factor $Q^2/K^2_{\perp max}$ when $K^2_{\perp max} > Q^2$, we see that we can write the cross section in the following symmetric form

$$d\sigma \sim \left[\prod_i \frac{dz_i}{z_i}\frac{dK^2_{\perp i}}{K^2_{\perp i}}\right]\frac{1}{K^2_{\perp max}} \tag{38}$$

where the photon is included in the product. Here $K_{\perp max}$ can correspond to the photon ("normal DIS"), to the last parton in the chain (photon-gluon fusion) or to some earlier exchanged gluon in the chain (hard resolved photon scattering).

—

Our conclusions from this section are that within the Linked Dipole Chain model it is possible to generalize the result of the CCFM model and obtain a unified description of these different event types. We also conjecture that it is possible to include subleading terms and quarks in the chain, using the splitting functions $P(z)$. We note that experience from e^+e^--annihilation has shown that for a good description of experimental results, it is essential that the hardest gluon is distributed in accordance with lowest order matrix elements, and not only in leading log approximation, [24]. Within the LDC Model it is also possible to construct a MC simulation program in which the hard scattering in a boson-gluon fusion or a hard parton-parton scattering is weighted by the proper matrix element.

6 Differential equations and anomalous dimensions

6.1 The differential equations

To conform with conventional notation we from now on use lowercase letters instead of capitals for gluon momenta. As discussed in the previous section, for fixed values of x and Q^2 the parton chain must end somewhere on the line AB (for $k^2_\perp < Q^2$) or on AC (for $k^2_\perp > Q^2$). Therefore the structure function $F(x, Q^2)$ can be expressed in terms of the nonintegrated structure function $\mathcal{F}(x, k^2_\perp)$ introduced above in the following way

$$F(x,Q^2) = \int \frac{dk^2_\perp}{k^2_\perp}\mathcal{F}(x', k^2_\perp) \quad \text{with} \quad x' = \begin{cases} x & \text{if } Q^2 > k^2_\perp \\ xk^2_\perp/Q^2 & \text{if } Q^2 < k^2_\perp \end{cases} \tag{39}$$

Here $x' = \prod z_i$ is the product of all the steps in the chain while $x \equiv x_{Bj} = Q^2/(2m\nu)$. (Note that we define $\mathcal{F}$ as a density in $\log(k^2_\perp)$, which differs from the notation $F \sim \int d^2k_\perp \tilde{F}$ in ref [6]. Thus we have the relation $\mathcal{F} = \pi k^2_\perp \tilde{F}$.)

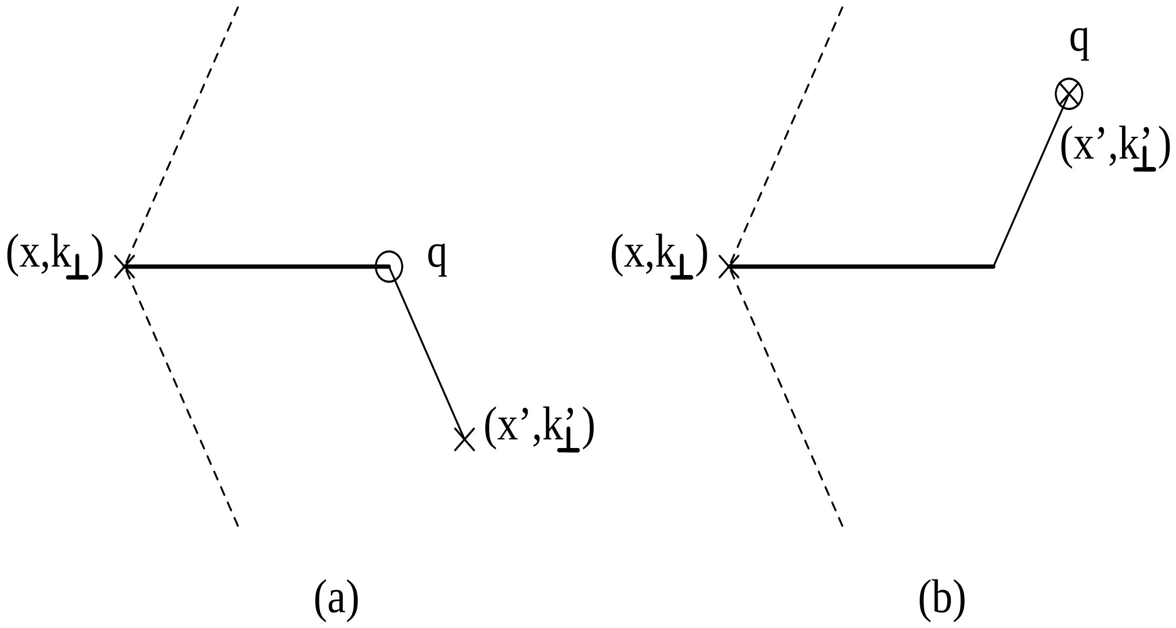

Figure 18: *The phase space limits for the last step leading to* $(x, k_\perp)$.

It is now straightforward to derive the following recursion relation, which describes the last step leading to $(x, k_\perp)$

$$\mathcal{F}(x, k_\perp^2) = \bar\alpha + \bar\alpha \int \frac{dx'}{x'} \int \frac{d^2 k'_\perp}{\pi q_\perp^2} \cdot \frac{k_\perp^2}{{k'}_\perp^2} \cdot \mathcal{F}(x', {k'}_\perp^2) \cdot \theta[q_\perp - \min(k'_\perp, k_\perp)] \cdot \theta[x' - \max(x, x\frac{{k'}_\perp^2}{k_\perp^2})] \quad (40)$$

where $\vec{q}_\perp = \vec{k'}_\perp - \vec{k}_\perp$.

The first θ-function follows because emissions with $q_\perp < \min(k'_\perp, k_\perp)$ are treated as final state radiation and are therefore not included in the primary chain. We note in particular that this implies that there is no collinear singularity for $q_\perp = 0$. The second θ-function is a consequence of the ordering in q_- and K_-, which follows from the constraint $k_\perp^2 > z \cdot q_\perp^2$ (eq (24)). Therefore, for fixed $k_\perp$ and x, the point corresponding to $k'_\perp$ and x' must lie to the right of the dashed line in fig 18, which for $k'_\perp > k_\perp$ corresponds to the constraint $k_\perp^2 > (x/x') \cdot {k'}_\perp^2$. (This implies that the $k_\perp^2$-integral in eq (39) is limited to the region $k_\perp^2 < Q^2/x$.)

We note in particular the fact that $\mathcal{F}$ only depends on the two variables x and $k_\perp^2$. This is in contrast to the corresponding function in the CCFM formalism, where the last step $k_{n-1} \to q_n + k_n$ also depends upon $q_{\perp(n-1)}$ and z_{n-1}, due to the angular ordering constraint $q_{\perp n} > z_{n-1} q_{\perp(n-1)}$ (cf also ref [25]). In our formalism there is no such dependence because the primary gluons are ordered both in q_+ and q_-, which also automatically implies an ordering in rapidity or angle. This is a considerable simplification when solving the equation.

An integration over the angle ϕ between $\vec{k'}_\perp$ and $\vec{k}_\perp$ in eq (40) gives

$$\int \frac{d\phi}{2\pi q_\perp^2} \theta(q_\perp - \min(k'_\perp, k_\perp)) = \begin{cases} \frac{1}{k_\perp^2} h({k'}_\perp^2/k_\perp^2) & ;\ k'_\perp < k_\perp \\ \frac{1}{{k'}_\perp^2} h(k_\perp^2/{k'}_\perp^2) & ;\ k'_\perp > k_\perp \end{cases} \quad (41)$$

where

$$h(a) = \frac{1}{1-a}\left[1 - \frac{2}{\pi} arctan\left(\frac{1+\sqrt{a}}{1-\sqrt{a}}\sqrt{\frac{2\sqrt{a}-1}{2\sqrt{a}+1}}\right)\theta(a-\frac{1}{4})\right] \quad ; \quad 0 < a < 1 \tag{42}$$

Taking the derivative of eq (40) we then get the differential equation

$$\frac{\partial \mathcal{F}(x,k_\perp^2)}{\partial(\log(1/x))} = \bar{\alpha}\left[\int^{k_\perp^2}\frac{dk_\perp'^2}{k_\perp'^2}\mathcal{F}(x,k_\perp'^2)\cdot h(k_\perp'^2/k_\perp^2) + \int_{k_\perp^2}\frac{dk_\perp'^2}{k_\perp'^2}\frac{k_\perp^2}{k_\perp'^2}\mathcal{F}(x\frac{k_\perp'^2}{k_\perp^2},k_\perp'^2)\cdot h(k_\perp^2/k_\perp'^2)\right] \tag{43}$$

To leading order in $\log(k_\perp^2)$ the ratio $k_\perp'^2/k_\perp^2$ is much different from unity, and the function h is close to 1. The first term is the DGLAP contribution where $k_\perp$ is increased in the last step. The second contribution contains the posssibility that $k_\perp$ is decreasing, $k_\perp < k_\perp'$. Then one has "to pay" first by the factor $k_\perp^2/k_\perp'^2$ and secondly because the x'-region in eq (40) is bounded by $x' > x \cdot k_\perp'^2/k_\perp^2$.

We note that for $q_\perp < k_\perp'$ we have $k_\perp' \approx k_\perp$, and therefore we have the following approximate relation

$$\frac{\mathcal{F}(x,k_\perp'^2)/k_\perp'^2}{q_\perp^2}\cdot\theta(q_\perp - k_\perp') \approx \frac{\mathcal{F}(x,k_\perp'^2)/k_\perp'^2 - \mathcal{F}(x,k_\perp^2)/k_\perp^2\cdot\theta(k_\perp - q_\perp)}{q_\perp^2} \tag{44}$$

If we insert this into eq (40), we obtain the same recursion relation as ref [6] and the differential equation

$$\frac{\partial \mathcal{F}(x,k_\perp^2)/k_\perp^2}{\partial(\log(1/x))} = \bar{\alpha}\int\frac{d^2k_\perp'}{\pi q_\perp^2}\left[\frac{\mathcal{F}(x',k_\perp'^2)}{k_\perp'^2} - \frac{\mathcal{F}(x,k_\perp^2)}{k_\perp^2}\cdot\theta(k_\perp - q_\perp)\right] \tag{45}$$

where $x' = \max(x, x\cdot\frac{k_\perp'^2}{k_\perp^2})$.

The derivation in ref [6] and our derivation of eqs (43) and (45) are accurate to double leading log approximation. In ref [26] it is demonstrated that although the results for exclusive final states is only correct to double log approximation, the result in eq (45) for the *inclusive* reaction is, for non-running α_s, actually correct to leading order in $\log(1/x)$, but to all orders in $\log(k_\perp^2)$.

The difference between $x' = x\cdot\frac{k_\perp'^2}{k_\perp^2}$ and x in eq (43) or eq (45) is only subleading in $\log(1/x)$. If this difference is neglected, we see that eq (45) is transformed into the Lipatov equation

$$\frac{\partial \mathcal{F}(x,k_\perp^2)/k_\perp^2}{\partial(\log(1/x))} = \bar{\alpha}\int\frac{d^2k_\perp'}{\pi q_\perp^2}\left[\frac{\mathcal{F}(x,k_\perp'^2)}{k_\perp'^2} - \frac{\mathcal{F}(x,k_\perp^2)}{k_\perp^2}\cdot\theta(k_\perp - q_\perp)\right] \tag{46}$$

As we will see in the next subsection, the difference between eqs (43) and (45) is numerically small (and actually less important than subleading terms in $\log(1/x)$). We believe that our formalism with linked dipoles is physically appealing. It is clearly visible how the collinear singularities are absent in the primary dipole chain (the initial state radiation in our formalism) and thus in the inclusive cross section (cf eq (40)), while they are present in the final state radiation in the same way as in e^+e^- annihilation, and thus present in the cross section for exclusive final states. Furthermore in our formalism a running coupling constant, α_s, can be naturally introduced, and because the links in the dipole chain correspond to larger steps in $\log(1/x)$, ie larger values of $\log(1/z)$, we can conjecture that subleading terms in $\log(1/x)$ are less important. In a future publication we want to study to what extent they can be accounted for by replacing the pole term $1/z$ by the relevant splitting functions $P(z)$.

We also note that the absence of the noneikonal form factors and the negative terms in eq (45) or eq (46) makes our formalism suitable for MC simulations. Instead of the infinite subtraction for $k'_\perp = k_\perp$ in eqs (45, 46) we have in eq (43) a finite subtraction within the region $1/2 < k'_\perp/k_\perp < 2$. This implies that the kernel in eq (43), and the corresponding weights in an iterative solution, are always positive, which greatly simplifies a MC treatment both of the structure function and of final state properties (cf ref [20]).

To understand the qualitative features of our model it is interesting to study a further approximation. Within the leading $\log(k_\perp^2)$ approximation, the factor $q_\perp^2$ in the denominator in eq (40) equals $\max(k_\perp^2, k_\perp'^2)$. We can then separate the $k'_\perp$ integral in eq (40) into three regions, corresponding to $k'_\perp \ll k_\perp$, $k'_\perp \gg k_\perp$ and $k'_\perp \approx k_\perp$. If expressed in the variables $\kappa = \log(k_\perp^2)$ and $L = \log(1/x)$ this gives the following simple result

$$\mathcal{F}(L,\kappa) = \bar{\alpha} + \int_0^\kappa \bar{\alpha} d\kappa' \int_0^L dL' \mathcal{F}(L',\kappa') + \int_\kappa^L \bar{\alpha} d\kappa' \exp\left[\kappa - \kappa'\right] \int_0^{L+\kappa-\kappa'} dL' \mathcal{F}(L',\kappa') - \bar{\alpha} A \int_0^L dL' \mathcal{F}(L',\kappa) \quad (47)$$

or the differential equation

$$\frac{\partial \mathcal{F}}{\partial L} = \int^\kappa \bar{\alpha} d\kappa' \mathcal{F}(L,\kappa') + \int_\kappa \bar{\alpha} \exp\left[-(\kappa'-\kappa)\right] d\kappa' \mathcal{F}(L-\kappa'+\kappa,\kappa') - A\bar{\alpha}\mathcal{F}(L,\kappa) \quad (48)$$

As before the first term is the DGLAP contribution, the second a contribution with a decreasing $k_\perp$ while the last term is a finite contribution which accounts for the extra suppression from the θ-function when $k'_\perp \approx k_\perp$. As discussed in next subsection this contribution can be adjusted so as to give the same anomalous dimension as eq (43), (45) or (46).

6.2 The anomalous dimensions

Finally let us study some properties of the anomalous dimensions. We will here only study the situation with a constant α_s, and postpone considerations on a running coupling constant to a future publication. Define the moments $\mathcal{F}_N$ according to

$$\mathcal{F}_N(k_\perp^2) = \int x^{N-1} \frac{dx}{x} \mathcal{F}(x, k_\perp^2) \quad (49)$$

and the anomalous dimension γ_N such that

$$\mathcal{F}_N(k_\perp^2) \propto (k_\perp^2)^{\gamma_N} = e^{\gamma_N \kappa} \tag{50}$$

Insertion into the Lipatov equation (46) gives the wellknown result

$$1 = \frac{\bar{\alpha}}{N-1}\chi(\gamma_N) \equiv \frac{\bar{\alpha}}{N-1}(g(\gamma_N) + g(1-\gamma_N)) \tag{51}$$

where

$$g(\gamma) = \int_0^1 \frac{da}{1-a}(a^{\gamma-1} - 1) = \psi(1) - \psi(\gamma) \tag{52}$$

Here ψ is the Euler function and the terms $g(\gamma)$ and $g(1-\gamma)$ correspond to contributions from $k'_\perp < k_\perp$ and $k'_\perp > k_\perp$ respectively. The function $\chi(\gamma)$ is symmetric around $\gamma = 1/2$ and therefore, for fixed N, eq (52) has two solutions γ_N and $1-\gamma_N$.

When N takes a value N_{sing} such that these solutions coincide at $\gamma = 1/2$, we obtain a "pinch singularity" in the inverse transforms. Thus N_{sing} is given by the relation

$$N_{sing} - 1 = 2\bar{\alpha} g(1/2) = 4\bar{\alpha}\log(2) \equiv \lambda \tag{53}$$

which implies the asymptotic behaviour

$$\mathcal{F} \sim x^{-\lambda} \tag{54}$$

For $\bar{\alpha} = 0.2$ we have $\lambda \approx 0.55$

If we instead use eq (45), and thus avoid the approximation $x' = x \cdot \frac{k_\perp'^2}{k_\perp^2} \approx x$, we find in the same way the result

$$1 = \frac{\bar{\alpha}}{N-1}(g(\gamma_N) + g(N-\gamma_N)) \tag{55}$$

with the same function $g(\gamma)$. We see that we now get a singularity when $\gamma_N = N/2$. Thus the dependence on x and $k_\perp$ is determined by the same parameter, and N_{sing} is determined by the relation

$$1 = \frac{\bar{\alpha}}{N_{sing}} \cdot 2g(N_{sing}/2) = \frac{\bar{\alpha}}{N_{sing}} \cdot 2\left[\psi(1) - \psi(\frac{N_{sing}}{2})\right] \tag{56}$$

which for $\bar{\alpha} = 0.2$ has the solution

$$N_{sing} \approx 1.31 \quad \text{or} \quad \lambda \approx 0.31 \tag{57}$$

We note that although the difference between eq (45) and eq (46) is subleading in $\log(1/x)$, it has a significant influence not only on the x-dependence, but also on the $k_\perp$-dependence of $\mathcal{F}(x, k_\perp)$.

If next we instead would start from eq (43) we find

$$1 = \frac{\bar{\alpha}}{N-1}\tilde{\chi}(\gamma_N) \equiv \frac{\bar{\alpha}}{N-1}\left[\tilde{g}(\gamma_N) + \tilde{g}(N-\gamma_N)\right] \tag{58}$$

with

$$\tilde{g}(\gamma) = \int_0^1 dah(a)a^{\gamma-1} \tag{59}$$

where h is defined in eq (42). Thus we have the same relation between the x- and the $k_\perp$-dependence, with a singularity for $\gamma_N = N/2$.

Numerically the difference between g and $\tilde{g}$ is not large and from eq (58) we find for $\bar{\alpha} = 0.2$

$$N_{sing} \approx 1.41 \quad \text{or} \quad \lambda \approx 0.41 \tag{60}$$

If finally we study the approximation in eq (48) we find in the same way

$$1 = \frac{\bar{\alpha}}{N-1}\left[\frac{1}{\gamma} + \frac{1}{N-\gamma} - A\right] \tag{61}$$

with the solution

$$N_{sing} = \frac{1}{2}\left[1 - \bar{\alpha}A + \sqrt{(1-\bar{\alpha}A)^2 + 16\bar{\alpha}}\right] \tag{62}$$

Thus e.g. for $A = 0.8$ eq (48) will give the same asymptotic behaviour as eq (43).

We end this section by noting that if there is a kinematical constraint as discussed in section 2, corresponding to an effective cut $\log(1/z) > a$, we get in the integrals in eq (52) or (59) the extra factor $e^{-(N-1)a}$ which will reduce the value of N_{sing} and λ. Further study of these effects will be postponed to future work.

7 Summary

We have briefly reviewed the usual treatment of Deep Inelastic Scattering reactions in terms of the DGLAP and BFKL mechanisms, which are meant to describe the properties of very large Q^2- and low x-moderate Q^2-interactions respectively. We exhibit a correction to the well-known BFKL power in the structurefunction, $x^{-\lambda}$, which turns out to considerably diminish λ.

We have reformulated and generalized the formalism for DIS developed by Ciafaloni and Catani et al [5, 6]. The result can be described in terms of a set of linked dipoles, which constitute the "initial state radiation". These dipoles emit "final state radiation" in a well-defined phase space region specified by the virtualities in the initial chain.

The formalism describes in a unified treatment both the usual QCD parton model, boson-gluon fusion events and hard subcollisions in resolved photon-proton scattering. It can also be applied to γ-proton and $\gamma\gamma$- interactions or hard hadron-hadron collisions.

We derive a new eqution for the hadronic structure functions. Just as the results in ref [5, 6], this equation contains contributions corresponding to both the BFKL and the DGLAP mechanisms, and we trace the differences between the approaches.

Acknowledgements

This work is supported in part by the EU Programme "Human Capital and Mobility", Network "Physics at High Energy Colliders", contract CHRX-CT93-0357 (DG 12 COMA).

Appendix

In this appendix we will formally demonstrate the equality in eq (28). Referring to fig 11 we introduce the following variables to specify the momenta q' to be summed over

$$\begin{cases} u = \log(q'_\perp/(z'Q_\perp)) \\ v = 2\log(z'/Z) \end{cases} \tag{A1}$$

where $Z = K_+/Q_+$ and $z' = q'_+/Q_+$. The interpretation of the parameters u and v is shown in fig 19, and the allowed region is given by

$$\begin{cases} 0 < u < L \equiv \log(1/z) \\ 0 < v < 2(L-u) \end{cases} \tag{A2}$$

Expressed in these variables the sum in eq (28) can be written in the form (note that the quantity A in eq (26) is given by $A = L^2$)

$$\sum_n \left[\prod_i^n \bar{\alpha} \int_0^L du_i \int_0^{2(L-u_i)} dv_i \cdot \theta(u_i - u_{i-1}) \cdot \theta(v_i - v_{i+1}) \cdot \exp\left[\bar{\alpha}(u_i - u_{i-1}) \cdot v_i\right] \right] \times \exp(-\bar{\alpha}A) \tag{A3}$$

Using the identity

$$\exp\left[\bar{\alpha}(u_i - u_{i-1}) \cdot v_i\right] = \sum_{m=0}^{\infty} \prod_k^m \bar{\alpha} \int_{u_{i-1}}^{u_i} du'_k \int_0^{v_i} dv'_k \cdot \theta(u'_k - u'_{k-1}) \tag{A4}$$

eq (A3) can be cast in the following form (For fixed N the variables U_J and V_J correspond to the different possibilities for the variables (u_i, v_i) and (u'_k, v'_k) with $n + m = N$, ordered

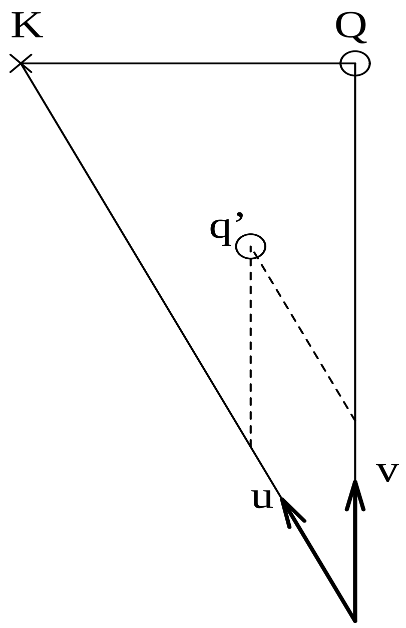

Figure 19: *Interpretation of the parameters u and v.*

according to the size of the u-variables.)

$$
\begin{aligned}
\exp(-\bar{\alpha}A)\cdot\sum_N\prod_J^N\bar{\alpha}\int_0^L dU_J\int_0^{2(L-U_J)} dV_J\cdot\theta(U_J-U_{J-1}) &= \\
\exp(-\bar{\alpha}A)\cdot\sum_N\frac{1}{N!}\cdot\prod_J^N\left[\bar{\alpha}\int_0^L dU_J\int_0^{2(L-U_J)} dV_J\right] &= \\
\exp(-\bar{\alpha}A)\cdot\exp(\bar{\alpha}A) &= 1
\end{aligned}
\tag{A5}
$$

References

[1] V.N. Gribov and L.N. Lipatov, Sov. J. Nucl.Phys 15 (1972) 438 and 675 ;
V.N. Gribov In *Proceedings of the XVII Winter School of the LNPI*, Leningrad

[2] N. Christ, B. Hasslacher and A.H. Mueller, Phys. Rev. D6 (1972) 3543

[3] G. Altarelli and G. Parisi, Nucl.Phys. B126 (1977) 298

[4] E.A. Kuraev, L.N. Lipatov and V.S. Fadin, Zh. Eksp. Teor. Fiz. 72 (1977) 373 [Sov. Phys. JETP 45 (1977) 199];
Ya.Ya. Balitsky and L.N. Lipatov, Yad. Fiz. 28 (1978) 1597 [Sov. J. Nucl. Phys. 28 (1978) 822]

[5] M. Ciafaloni, Nucl. Phys. B296 (1988) 49

[6] S. Catani, F. Fiorani and G. Marchesini, Phys. Lett. B234 (1990) 339; Nucl. Phys. B336 (1990) 18

[7] G. Gustafson, Phys. Lett. B175 (1986) 453;
G. Gustafson and U. Pettersson, Nucl. Phys. B306 (1988) 746;
B. Andersson, G. Gustafson and L. Lönnblad, Nucl. Phys. B339 (1990) 393

[8] L. Lönnblad, Comput. Phys. Commun. 71 (1992) 15

[9] For a review, see Yu.L. Dokshitzer, V.A. Khoze, A.H. Mueller and S.I. Troyan, Basics of Perturbative QCD (Editions Frontières, Gif-sur-Yvette, 1991)

[10]) Yu.L. Dokshitzer, Sov. Phys. JETP 46 (1977) 641

[11] B. Andersson, G. Gustafson and J. Samuelsson, Lund preprint, LU-TP 95-12

[12] B. Andersson, G. Gustafson, H. Kharraziha and J. Samuelsson, Lund preprint, in preparation

[13] A.H. Mueller, Nucl.Phys. B415 (1994) 373

[14] Ya.I. Azimov, Yu.L. Dokshitzer, V.A. Khoze and S.I. Troyan. Phys. Lett. B165 (1985) 147

[15] B. Andersson, G. Gustafson and C. Sjögren, Nucl. Phys. B380 (1992) 391

[16] B. Andersson, P. Dahlqvist and G. Gustafson, Phys. Lett. B214 (1988) 604

[17] B. Andersson, P. Dahlqvist and G. Gustafson, Z. Phys. C44 (1989) 455

[18] B. Andersson, P. Dahlqvist and G. Gustafson, Nucl. Phys. B328 (1989) 76

[19] G. Gustafson, A. Nilsson, Nucl. Phys. B355 (1991) 106;
G. Gustafson, A. Nilsson, Z. Phys. C52 (1991) 533

[20] G. Marchesini and B.R. Webber, Nucl. Phys. B238 (1984) 1;
B.R. Webber, Nucl. Phys. B238 (1984) 492

[21] G. Marchesini and B.R. Webber, Nucl. Phys. B310 (1988) 461

[22] A.H. Mueller, Phys. Lett. B104 (1981);
B.I. Ermolaev and V.S. Fadin, JETP Lett. 33 (1981) 269;
A. Bassetto, M. Ciafaloni, G. Marchesini and A.H. Mueller, Nucl.Phys.B207 (1982) 189

[23] B. Andersson, G. Gustafson and Hong Pi, Z.Phys. C57 (1993) 485

[24] M.H. Seymour, Zeit. Phys. C56 (1992) 161

[25] J. Kwieciński, A.D. Martin and P.J. Sutton, Durham preprint, DTP/95/22

[26] S. Catani, F. Fiorani, G. Marchesini and G. Oriani, Nucl. Phys. B361 (1991) 645